BRANZ

**External Research Report**

Report ER31 [2018]

# Novel hybrid damping devices and design techniques for damage-avoidance seismic response of low and medium-rise structures

G.W. Rodgers, F.G. Golzar, J.G. Chase, R. Kordani, G.A. MacRae, N.K. Hazaveh

Project LR0455

University of Canterbury, funded by the Building Research Levy

1222 Moonshine Road
RD1, Porirua 5381
Private Bag 50 908
Porirua 5240
New Zealand
branz.nz

Funded from the Building Research Levy

Cover page photo credit: Danica Nel, QuakeCoRE

Issue Date: 27/07/2018


ISSN: 2423-0839

# Novel hybrid damping devices and design techniques for damage-avoidance seismic response of low and medium-rise structures

G.W. Rodgers, F.G. Golzar, J.G. Chase, R. Kordani, G.A. MacRae, N.K. Hazaveh.

## Preface

Research investigating low-damage seismic design principles in low- to medium-rise structures is undertaken, with a focus on rocking structure demand prediction and energy dissipation devices. Experimental and analytical studies are undertaken on individual and hybrid combinations of energy dissipation components. System-level numerical modelling and experimental testing of low-damage seismic design structures is undertaken to assess the influence of different damping device designs.

## Acknowledgements

We are extremely grateful to BRANZ for funding to support this research. As a result of this funding, we were able to obtain co-funding from other funders to extend the scope of this research. As such, the research reported within this document was jointly funded by the BRANZ Building Research Levy, the Quake Centre, the NZSEE-EQC Ivan Skinner Award, QuakeCoRE, and the Natural Hazards Research Platform. This BRANZ funding was primarily used to support experimental testing, which contributed to the overall research programme undertaken with the co-funders/research partners.

# Table of Contents

# List of Figures:

# List of Tables:

# Introduction:

The necessity to create more resilient built infrastructure has been clearly identified in the wake of the Canterbury earthquakes. A substantial majority of Christchurch inner-city apartment buildings have been demolished due to damage suffered in these earthquakes. This type of high density urban housing is especially important as housing costs continue to rise and housing affordability becomes an even bigger problem for most New Zealanders. Land costs have been identified as the key contributor to the sharp increase in housing costs in the last decade (Affordability Feature, BRANZ Build 140). Therefore, developing more robust design methods for medium to high-rise structures that do not induce a significant price premium on initial build costs will help provide affordable, high density housing options. This outcome will also help alleviate the increased demand on transport corridors, as higher density housing options enable people to live closer to their employment and social activity locations.

Increasing population, rapidly increasing house prices and growing transport problems is leading increased demand for high density urban housing in NZ. While most of Canterbury's housing stock responded well to ground shaking in the Canterbury earthquakes (excepting those that suffered from land damage/liquefaction), low to medium rise apartments buildings are subject to much higher demands and consequently suffered much more damage in Christchurch. This type of structure will be one key to the further economically sustainable and cost-effective development of major NZ cities over the next 20 years as people seek efficient work/life/housing solutions in a more urbanised NZ.

Building structures with rocking connections/frames are becoming popular as a means of achieving low-damage construction in New Zealand. This approach is particularly true for low-rise (2-5 story) structures, which comprise a range of medium density apartment buildings. New Zealand has led the development of these systems, with the first of these being the Te Puni apartments building in Wellington in 2007 (Gledhill et al, 2008). Since then a number of rocking structures have been constructed from concrete, steel and timber systems in Wellington, Nelson and Christchurch.

However, a potential issue was identified with the design of these rocking/jointed building systems. More specifically, there has been a research challenge to develop robust design guidelines for the required strength of rocking frame buildings, to quantify the bending moment and shear force demand. One key aspect has been the different demand imposed upon rocking frame structures as the height/number of floors in the building increases and aspect ratio of the wall become more off-square.

These shortcomings have been identified in the low damage structure report to the Royal Commission on the Canterbury Earthquakes (Buchanan et al, 2011). Further discussions on a number of these issues and similar low-damage structural systems have been described by MacRae and Clifton (2013).

Overall, several issues with the rocking frame systems have been identified that need to be addressed to potentially facilitate wider uptake of these low-damage structural systems for a wide range of applications. In particular:

- Building response prediction, especially determining the moment and shear demands imposed upon the rocking frames from higher mode effects.
- Developing sufficient post-tensioning displacement response capacity
- Ensuring the rest of the structure (including floor and frame components) is not damaged nor restricts frame deformations.
- Attachment of non-structural elements and the prevention of non-structural damage
- The implications of impact loads induced during rocking on horizontal and vertical floor accelerations and the resulting effects of building contents

The building response prediction will consider the effect of different types of dissipaters on frame response. Prior research has been undertaken in this area to assess the demands on rocking frame structures. However, several key questions remain due to the simplified models used in these areas of research. Specifically, some prior research has used a simplified, lumped mass model, with a rotational spring at the base to approximate rocking. Conversely, the recent research of Steele and Wiebe (2014) have proposed simplified methods to approximate the demands that are imposed from higher mode effects on wall systems with high aspect ratios.

There is a need to further assess these areas of research and indicate whether the simplified design methods are appropriate, capture the important dynamics, and most importantly, whether they are conservative and safe. These methods need to be assessed in a probabilistic sense, considering not just average response metrics, but also assessing the likelihood of extreme responses, to ensure structural performance at all potential levels of demand.

Furthermore, the absence of large structural damage/plastic hinge formation removes a key method of earthquake response energy dissipation. Therefore, a range of potential low-damage and damage-free energy dissipation devices are considered, which can be used in combination with the rocking frame design method, to achieve an overall design solution that manages both peak response parameters such as displacement, while also resulting in a structure that is not heavily damaged as a result of the earthquake.

This report covers several areas of key research, presented in individual sections. Initially, the results of research into rocking frame force demand prediction is presented. Subsequently, hybrid damping devices are developed and experimentally tested, and their response characteristics captured in numerical models. Finally, the influence of damping devices on the system-level structural performance is then assessed through computational modelling and shake-table testing.

# Rocking Frame Force Demand Prediction

## Executive Summary

Understanding the force and moment demands imposed upon rocking walls/frames, including the influence of higher mode effects is investigated. Four design approximation methods are compared to estimate the force demand of a set of structural rocking walls of 4, 8, 12, 16, and 20 storey. Non-linear time history analysis (NTHA) using a finite element rocking wall model is performed using a suite of 20 earthquake records to examine these four approximation methods: 1) Steel Construction New Zealand (SCNZ): A modified modal analysis applied to the initial linear system. 2) Weighted Capacity Design (WCD): Simplified equations are derived to estimate higher mode forces of an equivalent pin-based structure. 3) Substitute structure (SS): Reduced first mode forces are combined with higher mode forces of an equivalent structure with the secant stiffness for non-linear elements. 4) The Wiebe method: Higher modes are derived from an equivalent shear beam structure and are combined with the reduced first mode. Also the influence of the strength reduction on the robustness of the approximation methods are studied using the 8 storey wall with moment reduction factors of R = 2, 5, 10, and 20.

It was found that the SCNZ method does not always provide a good estimation for moment envelope and can overestimate the shear envelope for the 20 storey wall. The WCD method slightly underestimates the median moment and shear demand but provides a robust and consistent approximation. However, this method is not included in current commercial software packages. The Wiebe method provides an almost perfect approximation of the median shear demand for all the cases, and robustly approximates the moment demand for 4 and 8 storey rocking walls, but is conservative by up to 50% for taller structures compared to the median result of the NTHA. Considering the scatter of the results, the Wiebe method is the most reliable approach. For alternative moment reduction factors, the Wiebe method and SS are still able to robustly approximate the force demand. Reduction in energy dissipation increased the shear and moment demand of the 8 storey wall by 20% and 30% respectively. A sensitivity analysis using multiple ground motion suites indicates that the results are largely independent of ground motion suite used and the viscous damping models.

## Introduction

The concept of structural rocking systems was introduced to limit the overturning base moment of structures and to provide supplemental damping and self-centring. These systems comply with the broad principles of the PRESSS systems (Priestley, 2000) and the damage avoidance design (DAD) philosophy (Rodgers et al., 2015) and can produce controlled, repeatable energy dissipation without sacrificing structural components, given the right supplementary damping.

The use of a controlled rocking system enables the control of the first mode response. However, the presence of higher modes in the response can greatly influence structural response of rocking systems (Wiebe et al., 2013b,a; Chancellor et al., 2014; Priestley et al., 2000; Acikgoz and DeJong, 2016) and their effects must to be considered in estimation of force and moment demands to ensure a damage-free and capacity-protected design. For structures with a non-linearity at the base, estimation of higher mode effects using modal analysis of the initial elastic

system can lead to an underestimation of force demands, as shown by Sullivan et al. (2008). Pennucci et al. (2015) studied the effect of higher modes in tall reinforced concrete walls with a plastic hinge at the base and has proposed two methods to predict the inelastic higher mode response. These two methods are used for comparative purposes to predict the force demand of structural rocking walls. Estimation of force demands in ductile structures has been a focus of a study by Wiebe and Christopoulos (2015) where simplified equations are proposed to obtain non-linear higher mode forces. These simplified equations have been used in Steele and Wiebe (2016) to predict the force response of a set of steel rocking frames where they provided a good approximation of force and moment demands.

Structural rocking walls are usually designed to remain elastic during the uplift and create a non-linear elastic response (Holden et al., 2003; Restrepo and Rahman, 2007). Therefore, a good approximation of higher mode effects is essential for a damage-free design of these systems where the structure must remain functional after a design level earthquake. This project aims to address the need by seeking answers to the following questions:

1. Which of the currently available design methods provides the best assessment of the force demand in rocking wall structures of various height?
2. How does the strength reduction factor at the base, $R = M_{fixed\text{-}base}/M_{rocking}$, influence the robustness of predictions from the design methods?
3. How does the choice of damping model or ground motion suite influence the response?
4. How does the percentage force contribution from post-tensioning and energy dissipation to the overall base moment at the onset of rocking affect the peak shear force and bending moment demand within the wall?

Answering these questions will provide an insight to key design aspects and dynamic behaviour of rocking walls. Four methods are selected to estimate the force demand of a set of structural post-tensioned rocking walls with energy dissipation devices. These methods are simple and easily applicable to walls, frame, frame-wall systems. Specifically, the methods are defined:

1) Steel Construction New Zealand (SCNZ) design guideline (Wiebe et al., 2015) suggests a modal combination rule where higher mode forces are added directly to the reduced first mode to determine the capacity design actions.
2) The Wiebe approach (Wiebe and Christopoulos, 2015), where modal contributions are derived from an analogy to a cantilever shear beam with uniform elasticity and mass and variable base fixity. The first 3 mode contributions are analytically defined:

$$V_{1,max} = 1.5\big(M_{b,max}/H\big)[1-(z/H)^2] \quad (1a)$$

$$V_{2,max} = 0.1265[S_a(T_1/3)](W_{trib}/g)|\cos 4.49(z/H) + 0.217| \quad (1b)$$

$$V_{3,max} = 0.0297[S_a(T_1/5)](W_{trib}/g)|\cos 7.73(z/H) - 0.1283| \quad (1c)$$

$$M_{1,max} = M_{b,max}[1 - 1.5(z/H) + 0.5(z/H)^2] \quad (2a)$$

$$M_{2,max} = 0.0282[S_a(T_1/3)](W_{trib}/g)H|\sin 4.49(z/H) + 0.976(z/H)| \quad (2b)$$

$$M_{3,max} = 0.00384[S_a(T_1/5)](W_{trib}/g)H|\sin 7.73(z/H) - 0.991(z/H)| \quad (2c)$$

Which can be combined to yield:

$$V_{max}(z) = V_{1,max}(z) + \sqrt{\left(V_{2,max}(z)\right)^2 + \left(V_{3,max}(z)\right)^2} \quad (3a)$$

$$M_{max}(z) = M_{1,max}(z) + \sqrt{\left(M_{2,max}(z)\right)^2 + \left(M_{3,max}(z)\right)^2} \quad (3b)$$

Where $M_{b,max}$ is the over-strength base overturning moment, $z$ is height above base, and $H$ is total height, $W_{trib} = g$ = the total tributary mass, and $Sa(T)$ = spectral acceleration at period $T$ in which the elastic first-mode period is $T_1$ and the second mode and third mode periods for the pinned-base shear beam are assumed to be $T_1/3$ and $T_1/5$, respectively. $M_{i,max}$ and $V_{i,max}$ are the moment and shear force of the *ith* mode respectively.

3) A substitute structure (SS) approach based on Pennucci et al. (2015) where a reduced response spectra is used to obtain the  rst mode forces and for higher modes a substitute structure with secant stiffness for non-linear members is utilised. In this method, which is in line with Priestley et al. (2007), damping is assumed to be equal to elastic damping for higher modes.
4) Weighted capacity design (WCD), as presented in Pennucci et al. (2015), where shear and moment envelopes for higher modes are computed using closed-form equations based on structural dynamics theory:

$$V_n(x) = m_{tot}\left[\rho c_{n,f}(x) Sa_{n,f} + (1-\rho) c_{n,p}(x) Sa_{n,p}\right] \quad (4a)$$

$$M_n(x) = m_{tot}\left[\rho d_{n,f}(x) Sa_{n,f} + (1-\rho) d_{n,p}(x) Sa_{n,p}\right] \quad (4b)$$

where $\rho$ is the weighting factor for fixity of the system (0 for pinned-base and 1 for fixed-base). Dynamics Force distribution parameters, c and d are presented in Table 1 and $Sa$ is the elastic spectral acceleration. Subscripts $p$ and $f$ denote pinned-base and fixed-base systems, respectively.

Capacity design force envelope shapes proposed by Pennucci et al. (2015) are shown in Figure 1. Base shear decreases linearly up to the mid-height and remains constant up to the roof level. Base moment increases linearly up to the mid-height and then decreases linearly to $0.8H$ where $M_{0.8H} = 0.8M_{mid}$ and linearly reduces to zero at the roof level. Therefore, mid-height and base design forces define the overall capacity envelope shapes.

*Table 1: Weighted Capacity Design (WCD) parameters*

| Fixed-base | Mode 1 | Mode 2 | Mode 3 | Mode 4 |
|---|---|---|---|---|
| $c(0)$ | 0.613 | 0.188 | 0.065 | 0.033 |
| $c(L/2)$ | 0.518 | 0.018 | 0.046 | 0.000126 |
| $d(L/2)$ | 0.151 | 0.0281 | 0.0002 | 0.0021 |

| Pinned-base | Mode 2 | Mode 3 | Mode 4 |
|---|---|---|---|
| $c(0)$ | 0.137 | 0.04 | 0.019 |
| $c(L/2)$ | 0.038 | 0.038 | 0.007 |
| $d(L/2)$ | 0.0347 | 0.0023 | 0.0002 |

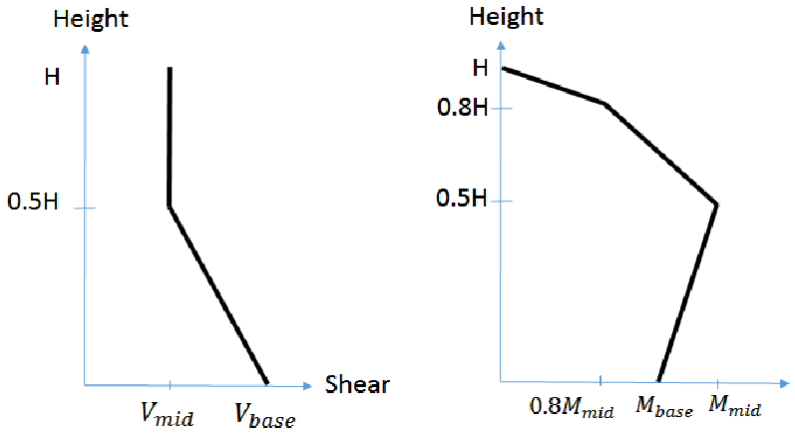


*Figure 1: Moment and Shear Capacity Envelopes*

To obtain the shear capacity design envelope, the first mode design base shear, $V_d$ is calculated from design procedures (Pennucci et al., 2009) and combined with higher mode shear forces defined:

$$V_{base} = \sqrt{V_d^2 + \sum_{i=2}^{n} V_i^2} \qquad (5a)$$

$$V(x) = \sqrt{(0.85V_d)^2 + \sum_{i=2}^{n} V_i^2} \qquad (5b)$$

where $V_{base}$ and $V(x)$ are the capacity design shear at the base and at any given height of the structure respectively. $V_i$ are higher mode shear forces and contribution of first mode design base shear to mid-height shear assumed to be $0.85V_d$.

# Methodology

## Structural Modelling

Finite element models are developed using MATLAB (MathWorks Inc, 2014) to represent structural rocking walls. The FE mesh for a typical 4 storey wall is shown in Figure 2 where the seismic mass of each floor is lumped at the corresponding node. Linear frame elements are utilised to represent the wall at each floor. The rigid footing is located on non-linear spring elements where, depending on the wall model, they can exhibit compression only, elasto-plastic and/or bi-linear behaviour to account for post-tensioning tendons and energy dissipaters. While simplified models do not capture all reaction mechanisms, they create a non-linear elastic response to model important characteristics and accurately obtain the global response of rocking systems.

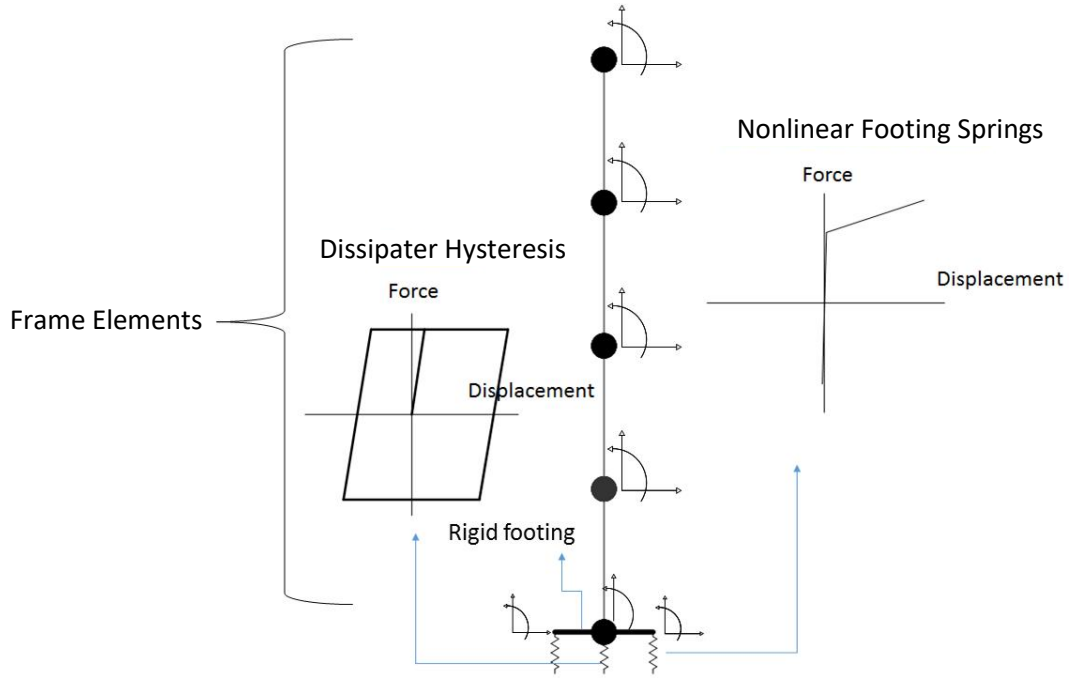


*Figure 2: Four storey rocking wall with post-tensioning and elasto-plastic damper, showing the elements with the associated hysteresis plots and degrees of freedom*

In this analytical and numerical study, inelastic deformation within the wall itself and changes in characteristics during dynamic loadings are not included. For example, toe crushing at the base and crack opening across a structural wall, can reduce the overall stiffness and influence the seismic response (Preti and Meda, 2015). A more sophisticated FEM is needed to study the influence of strength degradation on the force response of rocking walls. However, if the rocking wall is well detailed, such as through the use localised armouring in the regions of high contact forces near the rocking edges, inelastic action will be concentrated at the rocking base and this model will be reasonably accurate.

It is also important to investigate the force response of rocking walls under severe earthquake records as all the seismic design codes require some margin against collapse in seismic events with a return period greater than the design level. To ensure a robust capacity design, walls ductility demand must be characterised in case of severe events where there is a possibility of formation of plastic hinges across the rocking system height due to higher mode effects. It is assumed that the energy dissipation system behaves plastically during the post-uplift response regime and that the post-uplift stiffness is dependent upon the tendons only.

## Design of Rocking Post-tensioned Walls

A set of structural post-tensioned walls are adopted from Pennucci et al. (2009). Rocking walls provide only lateral force resistance and gravity loads are supported by gravity columns. Each rocking wall supports a seismic mass of 250 tonne per floor. It is also assumed that there is no mass or stiffness eccentricity and torsional eccentricity is neglected so the uncoupled lateral resisting systems can be modelled as a 2D system.

## Design of Energy Dissipation Devices and Post-Tensioning Tendons

Yielding, mild steel dissipaters and post-tensioning tendons together provide the minimum base moment for the rocking wall. The contribution to the base moment from the structural weight is neglected. Therefore, the total base moment at the onset of rocking is defined:

$$M_{base} = M_{ed} + M_{pt} \qquad (6)$$

where $M_{ed}$ and $M_{pt}$ are contributions to the rocking base moment from any added energy dissipation device and the post-tensioning tendons, respectively. In this study, a baseline value of Med = 0.45Mrocking will be used as a broadly acceptable value that provide a good tradeoff between static self-centering of the structure and a reasonable amount of energy dissipation.

A schematic diagram of the hybrid footing section of a wall is presented in Figure 3, where $l_w$ is the wall width and $C_c$, $T_{ed}$, and $T_{pt}$ are the forces induced by compression loads, supplemental energy dissipators, and post-tension cables respectively. Yield stress and the modulus of elasticity of the tendons and energy dissipaters are presented in Table 2. A variety of section parameters are used in this study to investigate the behaviour of rocking walls at different stiffness and frequencies. Each wall is designed for a specific strength reduction, R, at the base where:

$$M_{rock} = M_{fixed-base}/R \qquad (7)$$

$M_{rock}$ is the minimum base moment in which the energy dissipaters yield and the structure uplifts and begins to rock. $M_{fixedbase}$ is the base moment under the design force level, assuming a fixed-based footing. Due to the post-uplift stiffness of rocking joints, actual base moments under seismic loadings are greater than $M_{rock}$. Section parameters for all walls in the computational study in this research are presented in Tables 3-5.

*Table 2: Material Properties for the post-tensioning tendons and yield steel fuses/dissipaters*

| | *Post-Tensioned Tendons* | *Yielding Steel Dissipaters* |
|---|---|---|
| *Yield Stress, $f_y$ (MPa)* | *1560* | *300* |
| *Elastic Modulus , E (GPa)* | *195* | *200* |

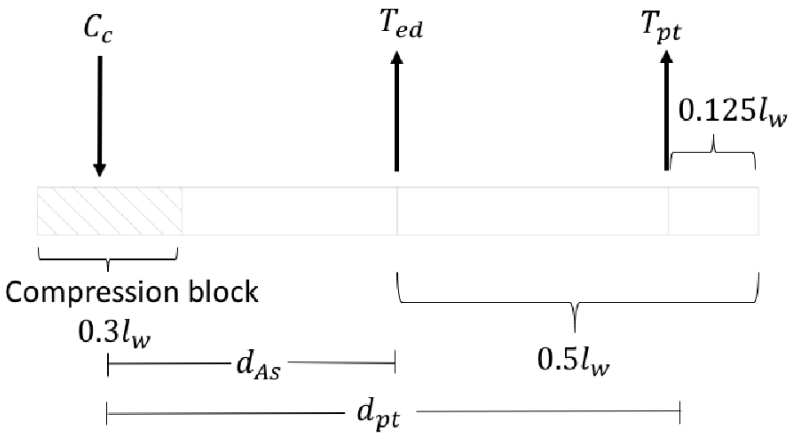


*Figure 3: Schematic diagram to indicate the assumed line of action of the hybrid footing at the rocking wall base*

In all tables, $l_w$ and $s_w$ are the length and width of the walls, respectively, $\rho_{mild}$ is the density of mild steel dissipaters, and $\rho_{pt}$ is the density of post-tensioning tendons. Equally, $f_{pt}/f_{pt\_y}$ is the post-tensioning ratio compared to yield strength of the post-tensioning tendons, $l_{ub}$ is the effective un-bonded dissipater length, and $d_{As}/l_w$ and $d_{pt}/l_w$ are the fractional eccentricity which define the dissipater and tendon location, as shown schematically in Figure 3.

*Table 3: Rocking wall parameters/section values for R = 5 and $M_{ed}$ = 0.45$M_{rock}$*

| | 4 story | 8 story | 12 story | 16 story | 20 story |
|---|---|---|---|---|---|
| $l_w$ (m) | 4 | 6 | 7.5 | 8 | 8.7 |
| $s_w$ (m) | 0.4 | 0.4 | 0.4 | 0.5 | 0.5 |
| $\rho_{mild}$ (%) | 1.47 | 1.63 | 1.52 | 1.3 | 1.3 |
| $\rho_{pt}$ (%) (each side) | 0.46 | 0.4 | 0.34 | 0.26 | 0.25 |
| $f_{pt}/f_{pt\_y}$ | 0.37 | 0.48 | 0.52 | 0.58 | 0.61 |
| $l_{ub}$ (m) | 0.2 | 0.4 | 0.6 | 0.6 | 0.6 |
| $d_{As}/l_w$ | 0.35 | 0.35 | 0.35 | 0.35 | 0.35 |
| $d_{pt}/l_w$ | 0.125 | 0.125 | 0.125 | 0.125 | 0.125 |

*Table 4: Section design values for the 8 storey wall with alternative strength reductions factors, using $M_{ed}$ = 0.45$M_{rock}$*

| | $R = 2$ | $R = 10$ | $R = 20$ |
|---|---|---|---|
| $l_w$ (m) | 6 | 6 | 6 |
| $s_w$ (m) | 0.4 | 0.4 | 0.4 |
| $\rho_{mild}$ (%) | 4 | 0.8 | 0.41 |
| $\rho_{pt}$ (%) (each side) | 1 | 0.2 | 0.1 |
| $f_{pt}/f_{pt\_y}$ | 0.48 | 0.48 | 0.48 |
| $l_{ub}$ (m) | 0.4 | 0.4 | 0.4 |
| $d_{As}/l_w$ | 0.35 | 0.35 | 0.35 |
| $d_{pt}/l_w$ | 0.125 | 0.125 | 0.125 |

*Table 5: Section design values for the 8 storey wall with alternative dissipation ratios, using constant force reduction factor of R = 5*

| | $M_{ed} = 0$ | $M_{ed} = 0.15M_{rock}$ | $M_{ed} = 0.3M_{rock}$ |
|---|---|---|---|
| $l_w$ (m) | 6 | 6 | 6 |
| $s_w$ (m) | 0.4 | 0.4 | 0.4 |
| $\rho_{mild}$ (%) | 0 | 0.54 | 1.09 |
| $\rho_{pt}$ (%) (each side) | 0.73 | 0.62 | 0.51 |
| $f_{pt}/f_{pt\_y}$ | 0.48 | 0.48 | 0.48 |
| $l_{ub}$ (m) | 0.4 | 0.4 | 0.4 |
| $d_{As}/l_w$ | 0.5 | 0.5 | 0.5 |
| $d_{pt}/l_w$ | 0.125 | 0.125 | 0.125 |

## Ground Motion Suites

All earthquake records of the medium suite design level of the SAC project (Somerville, 1997) are used to perform non-linear time history analysis (NTHA). It includes 10 different records with two orthogonal directions for each time history and represents ground motions with the probability of exceedance of 10% in 50 years. The ground motions are scaled to approximately conform to the 1997 NEHRP design spectrum for firm soil. Sensitivity of the analysis to different ground motion suites is also presented, where seismic response simulations of an 8 storey rocking wall are performed using FEMA far-field ATC (2009) records and acceleration histories form Vamvatsikos and Cornell (2001). FEMA and Vamvatsikos-Cornell records are scaled so that at the fundamental period of the 8 storey wall is (T = 0.91 s) their median spectrum matches the median of SAC suite as seen in Figure 4.

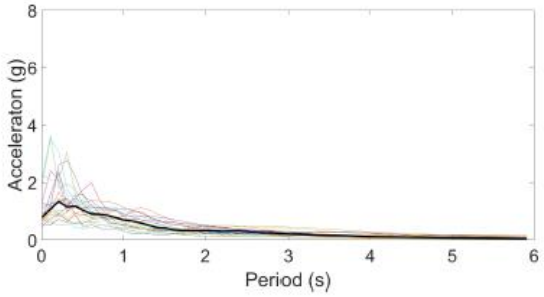


(a) SAC (Somerville, 1997)

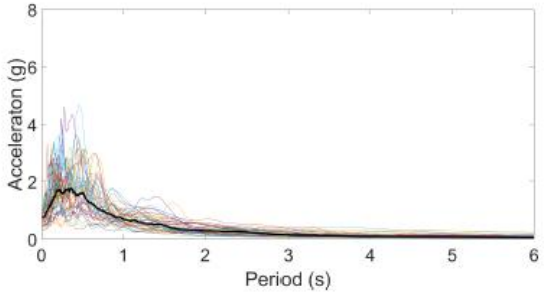


(b) FEMA (ATC, 2009)

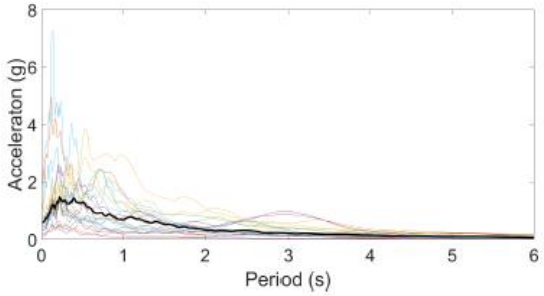


(c) Vamvat-Cornell (Vamvatsikos and Cornell, 2001)

*Figure 4: Spectral Acceleration response of all ground motions considered within this study.*

# Wall Behaviour Results and Discussions

## Effect of Structural Height

Design approximations for shear demand are compared with the numerical results of the NTHA using the SAC ground motion suite are presented in Figure 5. The Wiebe method provides an almost perfect match to the median results of NTHA. The SCNZ overestimated the shear demand for all the walls. This overestimation is more significant for taller structures and the modal combination method, which is used in SCNZ, has led to a conservative approximation. The SS method has slightly under-predicted the shear demand compared to the median, but has been consistent and reliable for all the rocking systems. Finally, WCD has underestimated the shear demand for all rocking structures. However, considering the simplicity of the procedure, it can be used to obtain preliminary results when dynamic analysis is likely to be performed.

Design approximations for moment demand are compared with the numerical analysis in Figure 6. A good approximation is obtained by the Wiebe method for the 4 and 8 storey systems. However, it overestimated the demand for taller structures. Finally, the SCNZ method provides a good moment estimation for 4 and 8 storey walls, but for taller structures is inaccurate and the modal combination employed in SCNZ has given a peculiar shape to the moment envelope for these taller structures. Both the SS method and WCD slightly under-estimate the moment demand except for the 4 storey wall, where WCD is conservative compared to the median. It is also worth noting that they have provided a consistent and reliable approximation despite being slightly non-conservative.

Results show that for rocking systems with 16 and 20 storey floors, median moment at mid-height can be substantially more than the base moment. Since structural rocking systems are usually designed to remain elastic under the design level, they may not be economically feasible solutions for tall earthquake resistant buildings. The cost of rocking systems should be economical, compared to conventional (ductile) designs and other seismic resistant methods like base isolation systems when the effect of higher modes are significant. Wiebe et al. (2013b) has proposed using multiple rocking joints to limit the higher mode effects in rocking systems, but this concept is not investigated in this research.

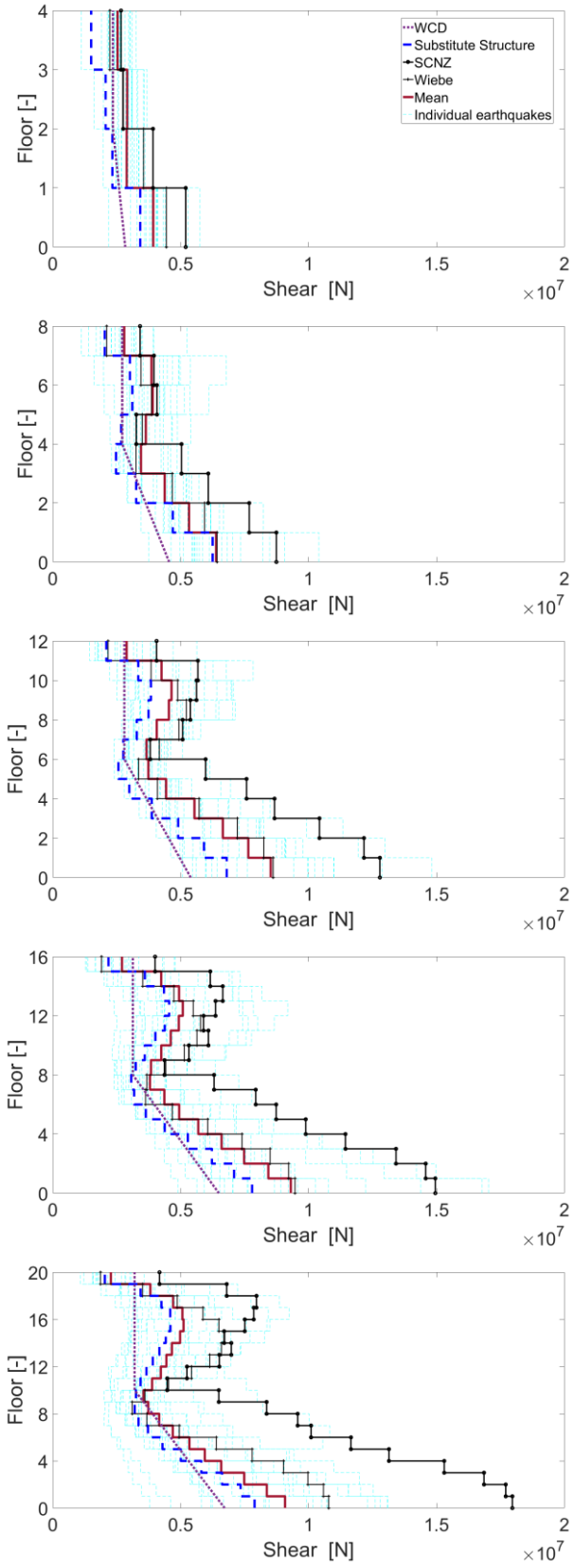


*Figure 5: Shear force comparison between NTHA results and predictions from different design methods*

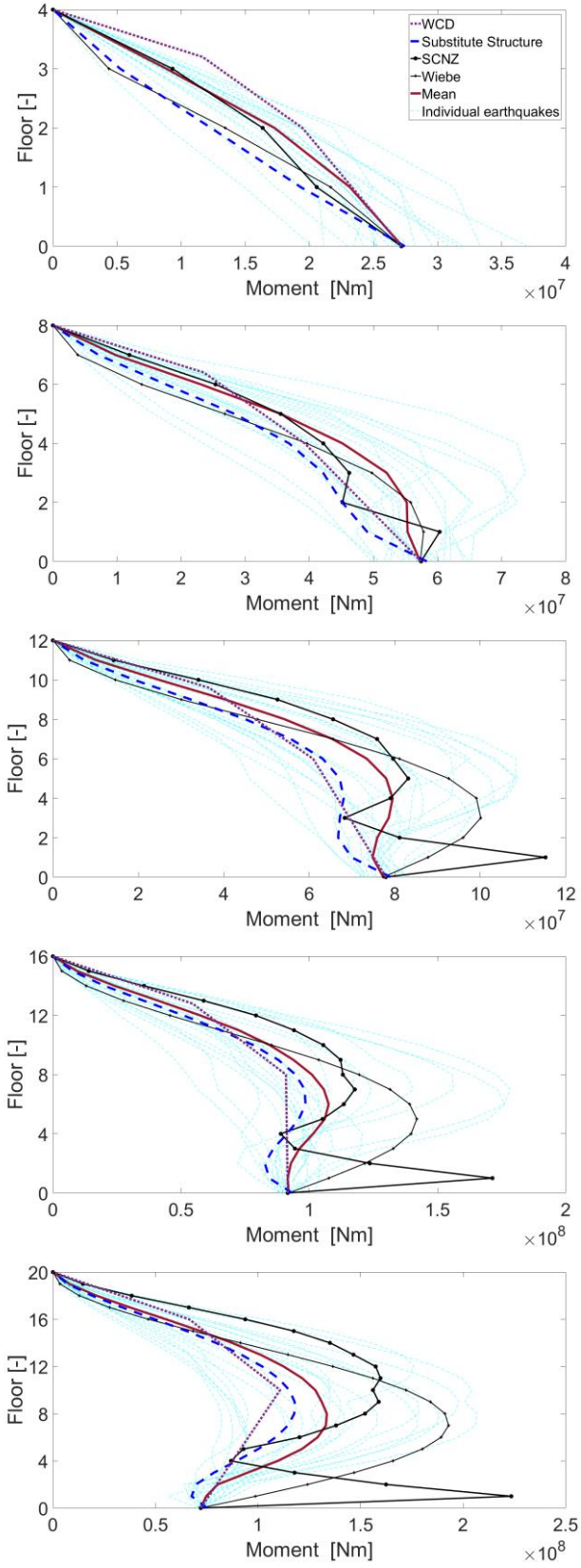


*Figure 6: Moment comparison between NTHA results and predictions from different design methods*

## Effect of Design Strength Reduction Factor, R

Rocking systems are generally designed to dissipate maximum seismic energy without sacrificing structural components and to maintain re-centring. In the design process for this type of system, the design strength reduction factor, $R$, indicates how the structure is performing relative to a traditional fixed-base system ($R = 1$) or a pin-based system ($R = \infty$). Usually practising engineers aim for choosing the highest strength reduction factor as long as the maximum drift and higher mode forces do not exceed the design limits and do not impose practical limitations. The rocking footing of the 8 storey wall is redesigned for different values of R to investigate the effect of design strength reduction on structural response.

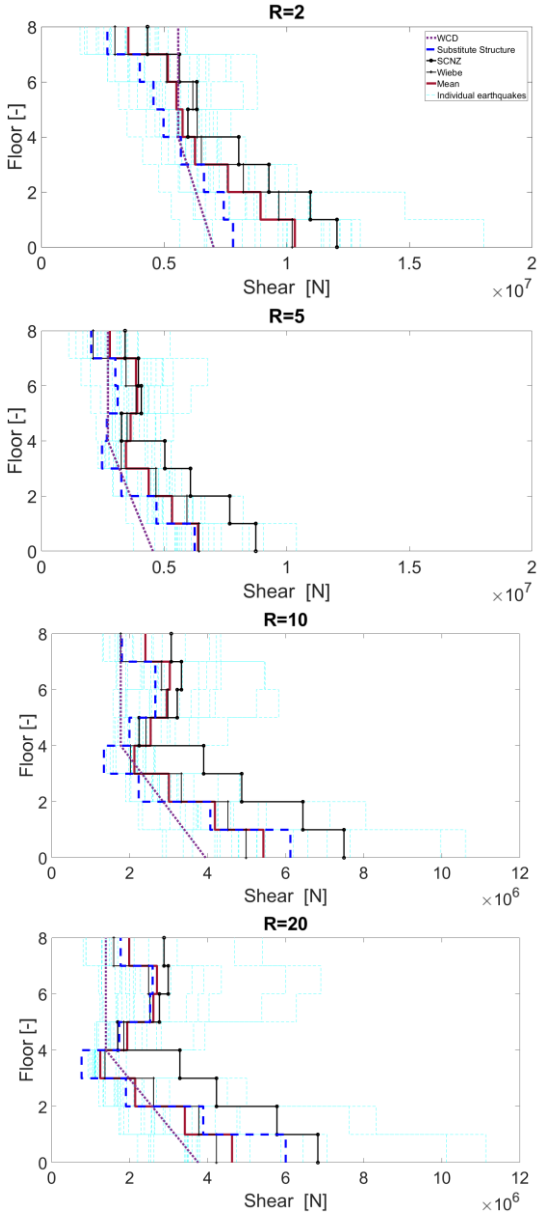


*Figure 7: Influence of force reduction factor (R) on the shear envelope and comparison with design predictions, using $M_{ed}$ = 0:45$M_{rocking}$*

Design approximations are compared with NTHA in Figures 7-8 in terms of shear and moment demand respectively. Strength reduction has almost no effect on the robustness of the design approximations, and the trend of results is similar to the previous section. Structures with strength reduction factors of $R$ = 10 and $R$ = 20 are very unlikely to be constructed in practice, but are presented here only for comparison purposes, to investigate the limiting case.

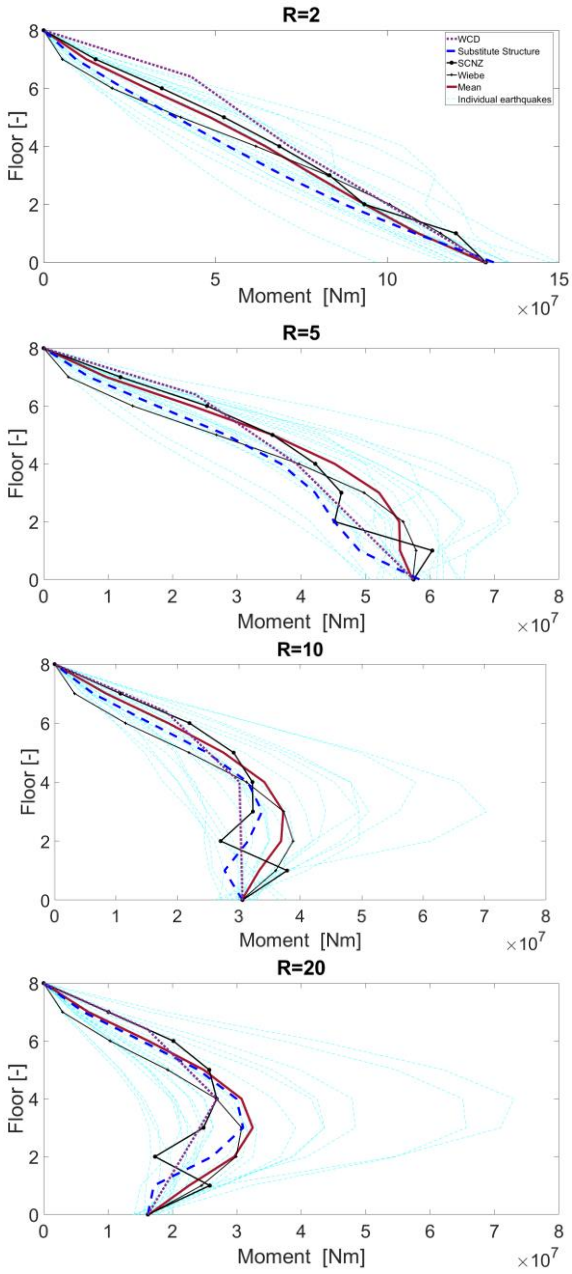


*Figure 8: Influence of force reduction factor (R) on the shear envelope and comparison with design predictions, using $M_{ed}$ = 0:45$M_{rocking}$*

## Effect of Ground Motion Suite Selection

The results previously present used the SAC ground motion suite as the input to the NLTHA. To investigate the influence of the ground motion records used and ensure that the results are not specific to those ground motions, additional suites are now used for comparison. Twenty-two records with two orthogonal directions for each history referred to as "Far-Field" records, are selected and normalized and scaled according to ATC (2009). Unscaled ground motions can be found in Haselton (2016). In addition, a suite of 20 ground motion records from Vamvatsikos and Cornell (2001) are scaled and used to examine the sensitivity of the analysis to ground motion suites. This sensitivity analysis is undertaken to ensure that conclusions are not drawn from a particular ground motion suite, which could potentially have unique frequency content or characteristics. Comparisons of the results are presented in Figure 9 where minimal dependency to the selection of earthquake records is observed. The median moment demands are closely similar throughout the wall, but vary slightly at the base. The shear force profiles show more variation, but the median values from the different suites is within approximately 15%. It can be concluded that the outcomes are generalisable and not specific to the ground motions selected for analysis.

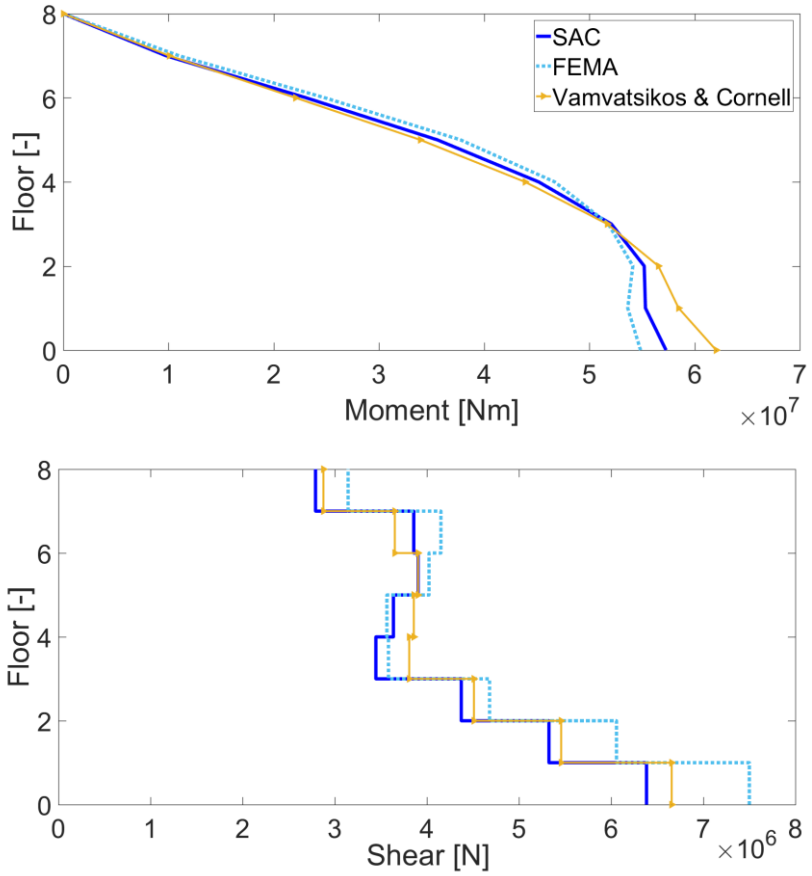


*Figure 9: Force demands of the 8 storey wall with R = 5 and Med = 0:45Mrocking for alternative seismic record suites (SAC, FEMA, and Vamvatiskos and Cornell)*

## Effect of inherent damping model on the analysis

The analysis presented in this paper used a modal viscous damping of 3% for the first mode and 5% for the higher modes. A modal damping matrix is computed using the initial stiffness of the rocking systems. Using reduced damping ratios for the first mode seems appropriate for structures with non-linearity at the base (rocking joint) as discussed in Smyrou et al. (2011). A second modal viscous damping model is developed to investigate the sensitivity of NTHA results to the inherent damping model utilised. In this model, the damping matrix is updated in each time-step based on the current stiffness matrix (tangent stiffness) and a damping ratio of 3% is assigned to all the modes. Median results are compared for two damping models in Figure 10 where the structural response of an 8 storey rocking wall with strength reduction of R = 5 and dissipation ratio of $M_{ed}$ = 0:45$M_{rocking}$ is presented.

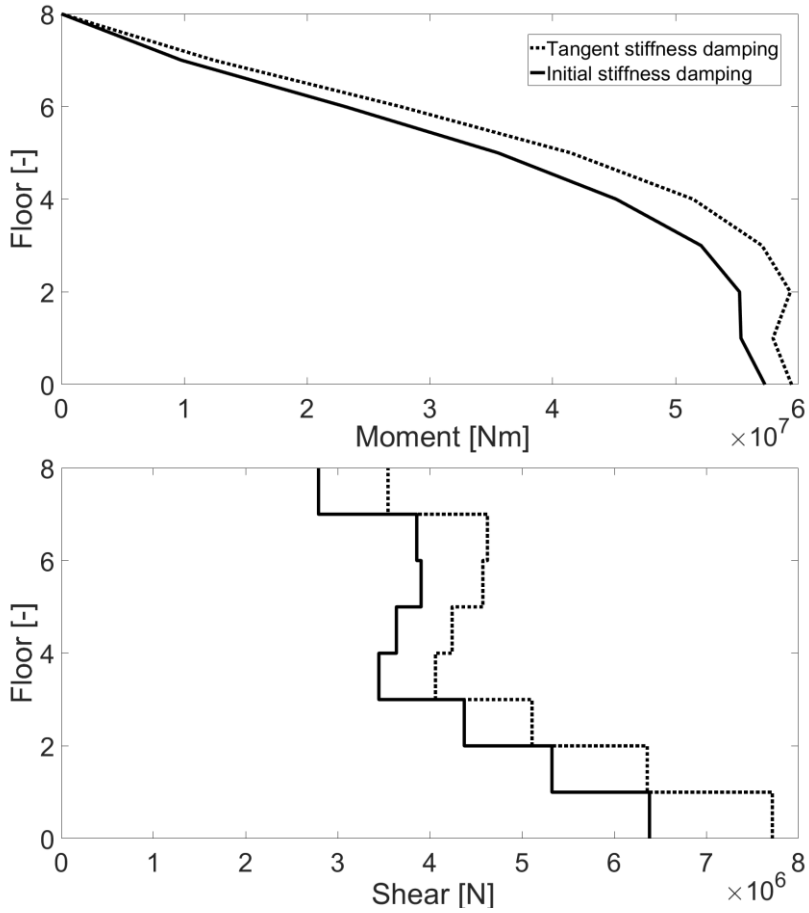


*Figure 10: Force demands of the 8 storey wall with alternative damping models.*

Using a tangent damping model is computationally more expensive and there is little experimental knowledge available about the accuracy of different damping models in the modelling of rocking walls. It can be seen in Figure 10 that assigning 3% of tangent damping to all the modes has increased the force envelop estimations but its effect is not significant. The difference is more pronounced for the shear envelope, but the differences in the moment envelope are minor.

## Effect of energy dissipation ratio on the analysis

NTHA is performed on an 8 storey rocking system with the strength reduction factor of R = 5, where the energy dissipation system and post-tensioned tendons contribute different amounts to the overall base moment. Due to the minimum post-uplift stiffness, ($M_{tot} = M_{rock}$) and the only design variable is the relative force contribution of energy dissipaters ($M_{ed}$) and tendons ($M_{pt}$) to the overall base moment, $M_{base}$, which is kept constant across the different suites. Force demands within the structure with different rocking joint configurations is presented in Figure 11, where there is a reduction in shear and moment demand through the application of energy dissipation.

It can be seen in Figure 11 that a decrease in the contribution of energy dissipation to the overall moment increases force and moment demand in the wall. The system with no dissipation devices, experienced an increase of up to 20% in moment demand and 30% in shear demand compared to the case with $M_{ed}$ = 0:45$M_{tot}$. As expected, the base moment remains that same for all cases as that was the design value that was kept constant across the different analyses. The maximum increase in force demands occurs for the case with no supplementary dissipation. The shear and moment demand obtained for this case can be used as upper bound values for design purposes.

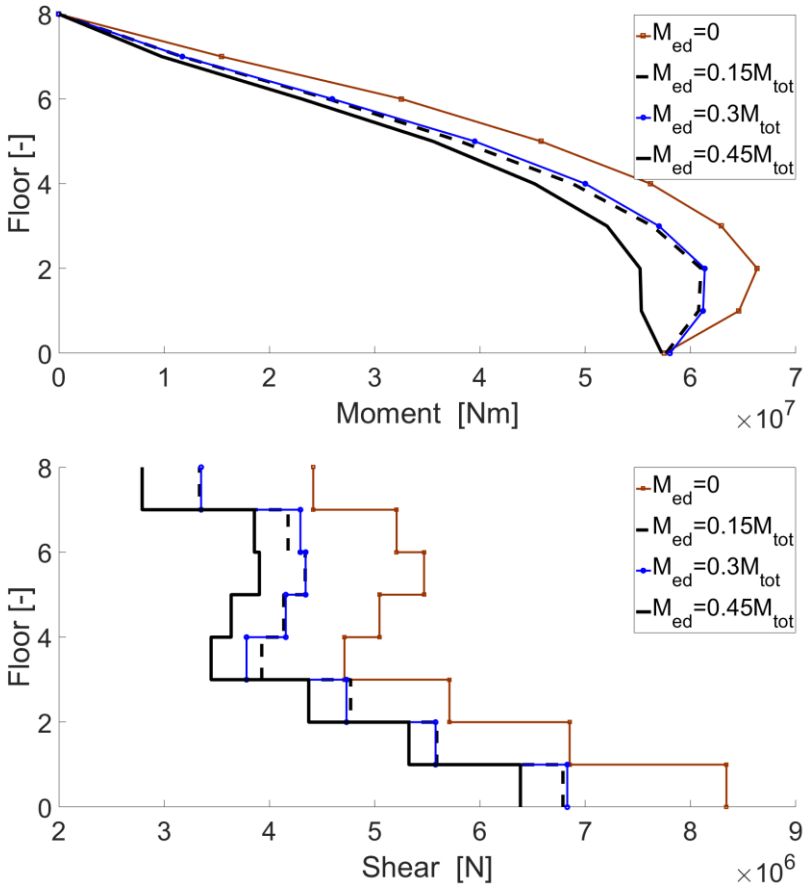


*Figure 11: Force demands of the 8 storey wall with alternative dissipation ratios*

# Conclusions

Moment and shear demands of structural rocking walls were investigated numerically through non-linear time-history analysis and the results for the shear force and bending moment compared to four different approximate design methods.

Based on the results presented within this study, it was concluded that:

1) The Wiebe and Substitute Structure methods provided the best approximation compared to the median results.
2) The robustness of these methods were independent to the structural height and strength reduction factor at the base. Overall, it was found that a good approximation of force response in rocking walls requires the obtaining of higher modes moment and shear forces using characteristics of the system after the onset of rocking. Therefore, methods like the SCNZ, that predict the force demand only based on the initial fixed base system can provide inaccurate estimations.
3) Parametric studies showed the choice of viscous damping models and ground motion suites did not significantly influence the response.
4) Finally, it was found that the force demand is effected by the energy dissipation ratio at the rocking joint. Reduction in supplementary energy dissipation led to an increase in force response. The increase was up to 20% for the shear demand and up to 30% for the maximum moment demand of the 8 storey rocking wall.

# References


Acikgoz, S. and DeJong, M. J. (2016). Analytical modelling of multi-mass flexible rocking structures. Earthquake Engineering & Structural Dynamics, (056):1{6.

ATC (2009). Quantification of building seismic performance factors. FEMA, (June):421.

Buchanan, A.H., Bull, D., Dhakal, R., MacRae, G., Palermo, A. and Pampanin, S. (2011) Base Isolation and Damage-Resistant Technologies for Improved Seismic Performance of Buildings. Royal Commission of Inquiry into Building Failure Caused by the Canterbury Earthquakes. 99pp.

Chancellor, N., Eatherton, M., Roke, D., and Akba, T. (2014). Self-Centering Seismic Lateral Force Resisting Systems: High Performance Structures for the City of Tomorrow. Buildings, 4(3):520{548.

Gledhill S.M., Sidwell G.K., and Bell D.K.. (2008) The Damage Avoidance Design of Tall Steel Frame Buildings - Fairlie Terrace Student Accommodation Project, Victoria University of Wellington, New Zealand Society of Earthquake Engineering Annual Conference, Wairakei, April 11-13.

Haselton, C. B. (2016). Research Databases. Chico, CA: California State University. http://www.csuchico.edu/structural.

Holden, T., Restrepo, J., and Mander, J. B. (2003). Seismic Performance of Precast Reinforced and Pre-stressed Concrete Walls. Journal of Structural Engineering, 129(3):286-296.

MacRae, G.A., and Clifton, G.C. (2013) Rocking Structure Design Considerations, Steel Innovations Conference 2013, Christchurch, New Zealand, 21-22 February

Pennucci, D., Calvi, G. M., and Sullivan, T. J. (2009). Displacement-Based Design of recast Walls with Additional Dampers Displacement-Based Design of Precast Walls with Additional Dampers. Journal of Earthquake Engineering, (February 2015):37-41.

Pennucci, D., Sullivan, T. J., and Calvi, G. M. (2015). Inelastic Higher-Mode Response in Reinforced Concrete Wall Structures. Earthquake Spectra, 31(3):1493-1514.

Preti, M. and Meda, A. (2015). RC structural wall with unbonded tendons strengthened with high-performance fiber-reinforced concrete. Materials and Structures, 48(1-2):249-260.

Priestley, M. J. N., Calvi, G., and M.J.Kowalsky (2007). Direct displacement-based seismic design. Proc. NZSEE Annual Conference., pages 1-23.

Priestley, M. J. N., Sritharan, S., Conley, J., and Pampanin, S. (2000). Preliminary Test Results from the PRESSS 5-Story Precast Concrete Building. PCI Journal, 44(6):42{67.

Restrepo, J. I. and Rahman, A. (2007). Seismic Performance of Self-Centering Structural Walls Incorporating Energy Dissipators. Journal of Structural Engineering, 133(11):1560-1570.

Rodgers, G. W., Mander, J. B., Chase, J. G., and Dhakal, R. P. (2015). Beyond Ductility: Parametric Testing of a Jointed Rocking Beam-Column Connection Designed for Damage Avoidance. ASCE Journal of Structural Engineering, 0733-9445/C4015006(10), pages 1-10.

Smyrou, E., Priestley, M. J. N., and Carr, A. J. (2011). Modelling of elastic damping in nonlinear time-history analyses of cantilever RC walls. Bulletin of Earthquake Engineering, 9(5):1559{1578.

Somerville, P. G. (1997). Development of ground motion time histories for phase 2 of the FEMA/SAC Steel Project.

Steele, T. C. and Wiebe, L. D. A. (2016). Dynamic and equivalent static procedures for capacity design of controlled rocking steel braced frames. Earthquake Engineering & Structural Dynamics, (056):1-6.

Sullivan, T. J., Priestley, M. J. N., and Calvi, G. M. (2008). Estimating the Higher-Mode Response of Ductile Structures. Journal of Earthquake Engineering, 12(3):456-472.

The MathWorks Inc (2014). MATLAB.

Vamvatsikos, D. and Cornell, C. A. (2001). Incremental Dynamic Analysis. Pages 1-23.

Wiebe, L. and Christopoulos, C. (2015). A cantilever beam analogy for quantifying higher mode effects in multi-storey buildings. Earthquake Engineering & Structural Dynamics, 44(11):1697-1716.

Wiebe, L., Christopoulos, C., Tremblay, R., and Leclerc, M. (2013a). Mechanisms to limit higher mode effects in a controlled rocking steel frame . 2 : Large-amplitude shake table testing. (September 2012):1069-1086.

Wiebe, L., Christopoulos, C., Tremblay, R., and Leclerc, M. (2013b). Mechanisms to limit higher mode effects in a controlled rocking steel frame. 1: Concept, modelling, and low-amplitude shake table testing. Earthquake Engineering & Structural Dynamics, 42(7):1053-1068.

Wiebe, L., Sidwell, G., and Gledhill, S. (2015). Design Guide for Controlled Rocking Steel Braced Frames. SCNZ 110:2015. Technical report, Steel Construction New Zealand Inc.

# Hybrid Damping Devices

## Executive Summary

Rocking structures that are designed to undergo a controlled rocking motion can be designed to provide different response characteristics at different levels of seismic hazard. The presence of an initial hold-down force through a mechanism such as post-tensioned tendons enables these structures to undergo a response similar to a fixed-base structure at low levels of seismic demand, but to initial a rocking response at higher levels of ground shaking. The rocking response will typically have a reduced stiffness and consequently have a longer period of vibration, which will usually correspond to a lower level of seismic demand, based upon a typical code-based design spectrum.

While these rocking structures have several key advantages, including the different response regimes at different levels of ground shaking, they also have the potential to deliver low-damage structural response. However, the absence of major damage to the primary structural elements (the absence of a plastic hinge) means that there is minimal hysteretic energy absorption. Consequently, rocking structures are at risk of increased displacement response due to an inherent lack of hysteretic energy dissipation from sacrificial structural damage. As such, they are particularly well suited to be augmented with supplemental damping devices to provide energy dissipation and limit the displacement response.

The ability to add reliable and robust energy dissipation to a structure is key to the an overall high-performance structural system that provides a response that does not have excessive displacement or acceleration response, but that also results leaves the structure free from any major damage.

Three key aspects of supplemental energy dissipation devices will be investigated within this study. These are viscous fluid dampers, lead extrusion dampers, and RingFeder ring springs. In addition, hybrid combinations of the RingFeder ring springs with both the viscous fluid dampers and the lead extrusion devices are investigated.

## Hybrid Damping Devices – Motivation

Energy dissipation devices can be broadly grouped into those that exhibit a velocity-dependent and velocity-independent force response. Simple mechanisms that use a yielding steel fuse or friction are typically velocity-independent, whereas viscous fluid dampers will usually exhibit a linear or non-linear force-velocity response, depending upon the working fluid. Viscous dampers that use fluids that exhibit Newtonian characteristics (such as simple oils and hydraulic fluid) will typically exhibit a linear force-velocity response. Conversely, fluid dampers that use a non-Newtonian fluid (such as high molecular weight silicone fluid) will typically exhibit a non-linear response behaviour.

Many structural engineers will prefer to use viscous fluid dampers that exhibit a non-linear force-velocity response profile, with a velocity exponent less than 1.0. Non-linear viscous fluid dampers have the notable advantage that the resistive force produced tends to saturate at high

velocity inputs. As a result, if the velocity imparted into a non-linear viscous fluid damper (velocity exponent < 1.0) is much higher than expected in design, the force produced may not be significantly higher than expected. However, with a linear viscous damper, a larger than expected velocity profile may induce much larger response forces and could potentially exceed the capacity of the damper connection elements.

By combining a velocity-dependent and velocity-independent energy dissipation, hybrid damping devices can produce an overall response profile that is relatively insensitive to the type of ground motion to which a structure is subjected. If a large, but far-field, ground motion occurs with long-duration but lower response velocity of the structure, the velocity-independent component of the damping device can provide a majority of the damping response. Conversely, if a large pule from a near-field ground motion excites the structure and imposed a larger demand, the velocity-dependent damping component can provide additional damping.

The viscous fluid dampers exhibit a velocity dependent response, with a velocity exponent in the range of 0.3-1.0, depending on the working fluid used. The lead extrusion devices exhibit a weakly velocity-dependent response, with the velocity exponent equal to approximately 0.1-0.12. Finally, the third energy dissipation component of the ring springs is load-rate independent and has no velocity dependence.

# Hybrid, Self-Centering Viscous Damper Testing

## Executive Summary

A prototype hybrid self-centring supplemental damper is designed and experimentally validated. The device combines a viscous damper with rate-dependent dissipation and a friction ring-spring with rate-independent dissipation and restoring force for re-centring. Experimental proof-of-concept tests input a range of displacement amplitudes and frequencies, for two levels of ring-spring pre-loads. Each component is also tested individually with the same displacement inputs to characterise and delineate their specific contributions. The prototype ring-spring has a maximum design force capacity of 26 kN while the viscous device shows a maximum 22 kN force at the highest input velocity of 330 mm/s. The individual and hybrid test results represent a combination of new options for energy dissipation in low-damage structures.

## Introduction

Fluid viscous dampers are fully passive dissipation devices that have proven effective in mitigating seismic structural response (Constantinou and Symans, 1992; Soong and Spencer, 2002). These devices can be used as supplemental retrofit devices in otherwise conventional structures. Their low complexity and quick response makes these viscous fluid devices a favourable supplemental dissipation option in earthquake-prone structures (Symans et al., 2008).

However, their lack of inherent re-centring capability can result in a permanent offset displacement. When coupled with the inelastic behaviour of the structure can lead to residual deformations (Barroso et al., 2003). To minimise this potential undesirable outcome, a dual hybrid supplemental damper consisting of viscous damper and ring-springs is designed to provide dissipation and re-centring restoring force. The hybrid device is experimentally validated in this research.

Ring-springs are friction based energy dissipation devices with self-centring restoring forces (Erasmus, 1988). A ring-spring essentially consists of a stack of inner and outer rings with tapered mating surfaces. When the stack is axially loaded, the inner rings undergo compression while the outer rings undergo tension. Thus, the rings slide along each other and reduce the overall length of the stack. When the force is removed, the rings slide back to their unloaded position due to the radial force within them. The friction at the sliding surfaces creates dissipation and the radial forces give the ring-spring re-centring capability. Possessing a dual dissipative and re-centring characteristic, ring-springs are a suitable addition to a viscous damper to create a re-centring dissipation device (Hill, 1995; Djojo et al., 2017).

This research addresses the design and experimental validation of a hybrid re-centring dissipation device. The hybrid device consists of a fluid viscous damper for dissipation and a friction ring-spring for re-centring. Such combination offers new options of low-damage dissipation techniques for uptake in industry where devices with similar behaviour have been successfully used to provide reliable earthquake protection ground motions (Mageba, 2013).

## Device Design – Viscous Device

The viscous device has a typical configuration consisting of a fluid filled steel housing and a shaft-piston coupling along its axis. The piston in fixed on the shaft and divides the fluid cavity into two parts. Shaft motion forces the damping fluid inside the housing to flow from one side to the other side of the piston through holes (orifices) located on the piston, imposing a level of resistance (damping) against shaft motion. The size and configuration of the orifices on the piston, as well as the piston area, determine the level of damping provided.

The piston in Figure 12 has a diameter of 101.6mm (4 in) and thickness of 20mm with 6×3.5mm orifices at 45mm PCD. The shaft is 31.75mm (1.25 in) in diameter and maximum device stroke is ±50 mm. SAE 80W-90 Castrol Axle oil with viscosity of 140 cSt at 40 degrees is used as the damping fluid for the viscous device. Endcaps are sealed using 14 M8 hexagonal cap screws and rubber seal rings around the endcap and using O-rings around the shaft to prevent leakage.

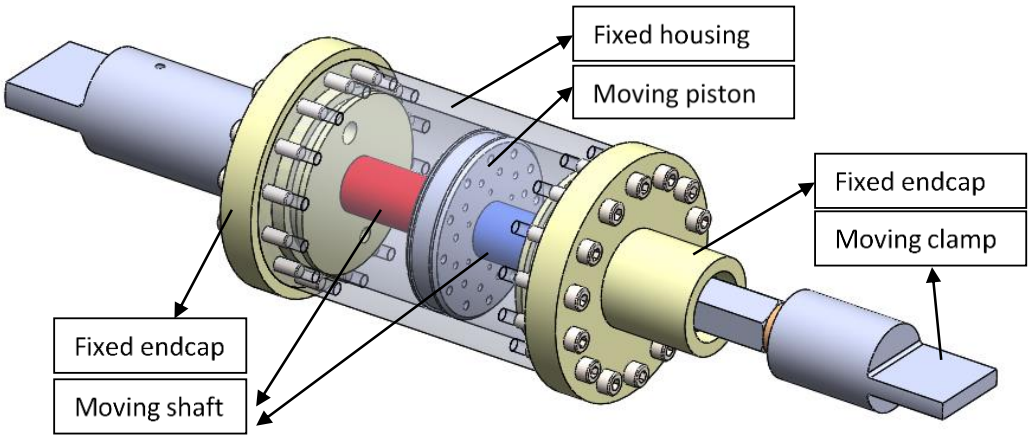


*Figure 12: Computer model of the prototype viscous device*

## Device Design – Friction-based Ring Springs

The ring-spring is shown in Figure 13. It consists of a ring stack mounted on an inner guide (shaft) and enclosed inside an outer guide (housing). Ringfeder (RINGFEDER, 2016) rings, with 19 inner rings and 20 outer rings of type 1205 were selected to form the ring stack. Figure 13 also shows the basic dimensions of the rings as well as the mating of outer and inner rings. The guides ensure axial deformation of ring column by preventing non-axial bulging/misalignment.

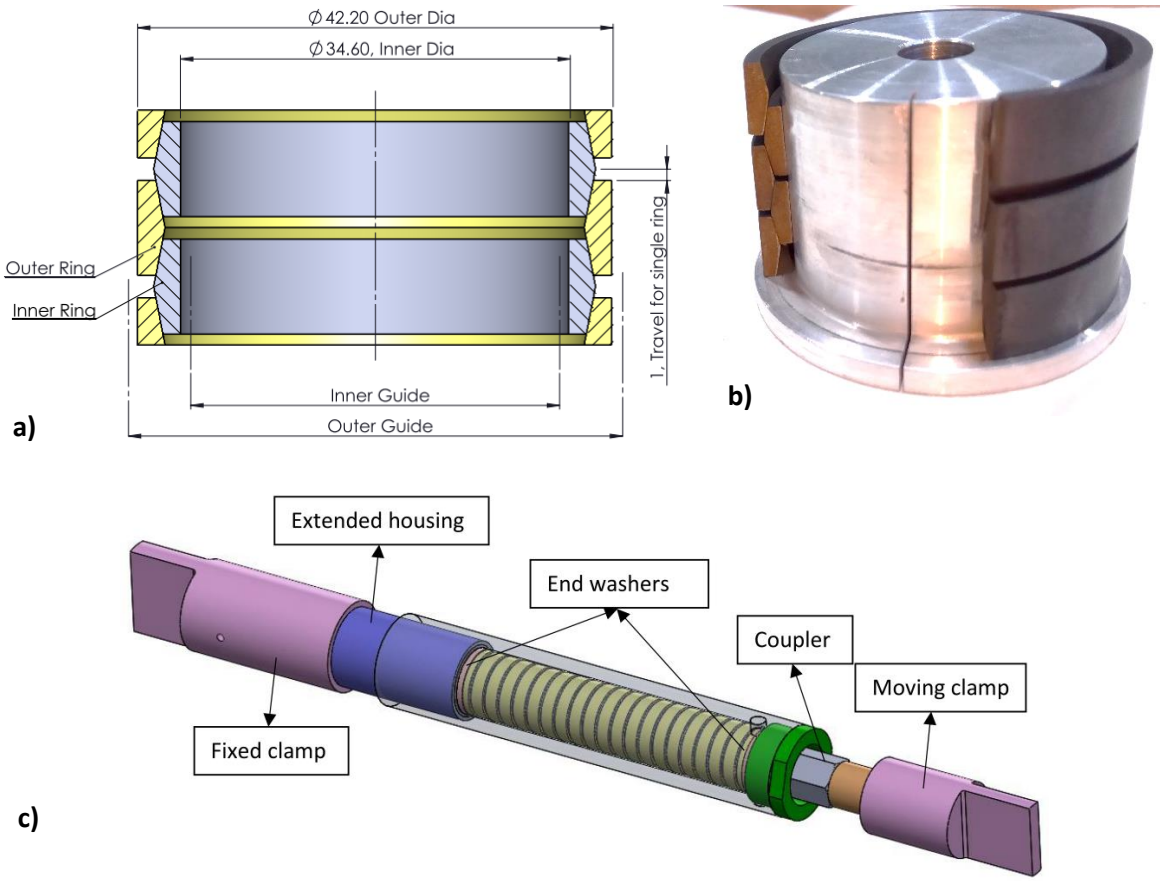


*Figure 13: Cross-sectional view of the rings (a, b) and prototype ring-spring device (c)*

In an unloaded condition, the stack is kept in place on the inner guide (shaft) using one washer at each end. As the shaft moves to one side due to an external displacement, it pushes one washer in the same direction while the other end washer is kept in place by a peripheral confinement on the housing, and thus compresses the ring stack. The washers can only move towards the rings to compress them and are otherwise blocked by threaded couplers screwed onto the shaft. This configuration ensures a double acting ring-spring; i.e. regardless of the direction of shaft motion, the ring stack will undergo the same deformation (compression) and thus the reaction force of the ring-spring will be symmetric with respect to its initial unloaded position (Figure 14).

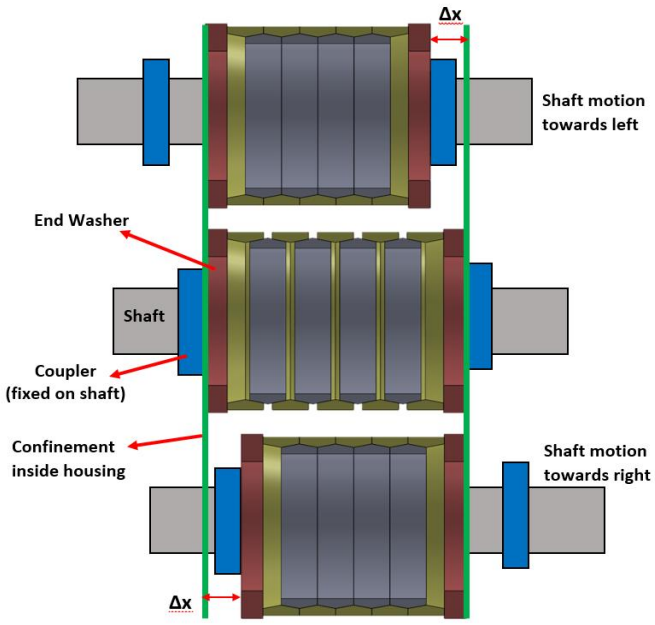


*Figure 14: Outer housing that induces compressive deformation of the ring-spring regardless of the direction of the input shaft motion*

To account for the change in the radial dimensions of the rings when the stack is axially loaded, the inner and outer guides are designed such that a measure of clearance is left between them and the rings. The radial clearance is 0.7mm between the rings and the outer guide (housing), and 2.0mm between the rings and inner guide (shaft). Thus, while the guides are tight enough to prevent misalignment, they provide sufficient clearance to accommodate the deformed ring dimensions.

To add preload to the ring-spring, the stack needs to be pre-compressed before mounting onto the hybrid device. The preload is added by placing extra washers on the ring stack before screwing threaded couplers on the shaft to reduce their nominal length and provide pre-compression. This process can be done to a specific preload using a load cell or one based on percentage of spring free length.

## Device Design – Hybrid Re-Centering Viscous Damper

The hybrid device consists of a parallel combination of the ring-spring and the viscous device. The design of the individual devices was optimised to allow easy integration of the two components. The same clamps (top and bottom) were mounted on the individual devices, as well as the hybrid device during each test.

To enable a parallel setup whereby each dissipative component undergoes the same displacement, the housing cylinder of the ring-spring was internally threaded to be screwed on the endcap of the viscous device (Figure 15). The shafts of the two components were connected using the threaded couplers (not shown in the figure). Thus, as the shaft moves within the hybrid device, the ring-spring displacement will be equal to the piston displacement inside the viscous device.

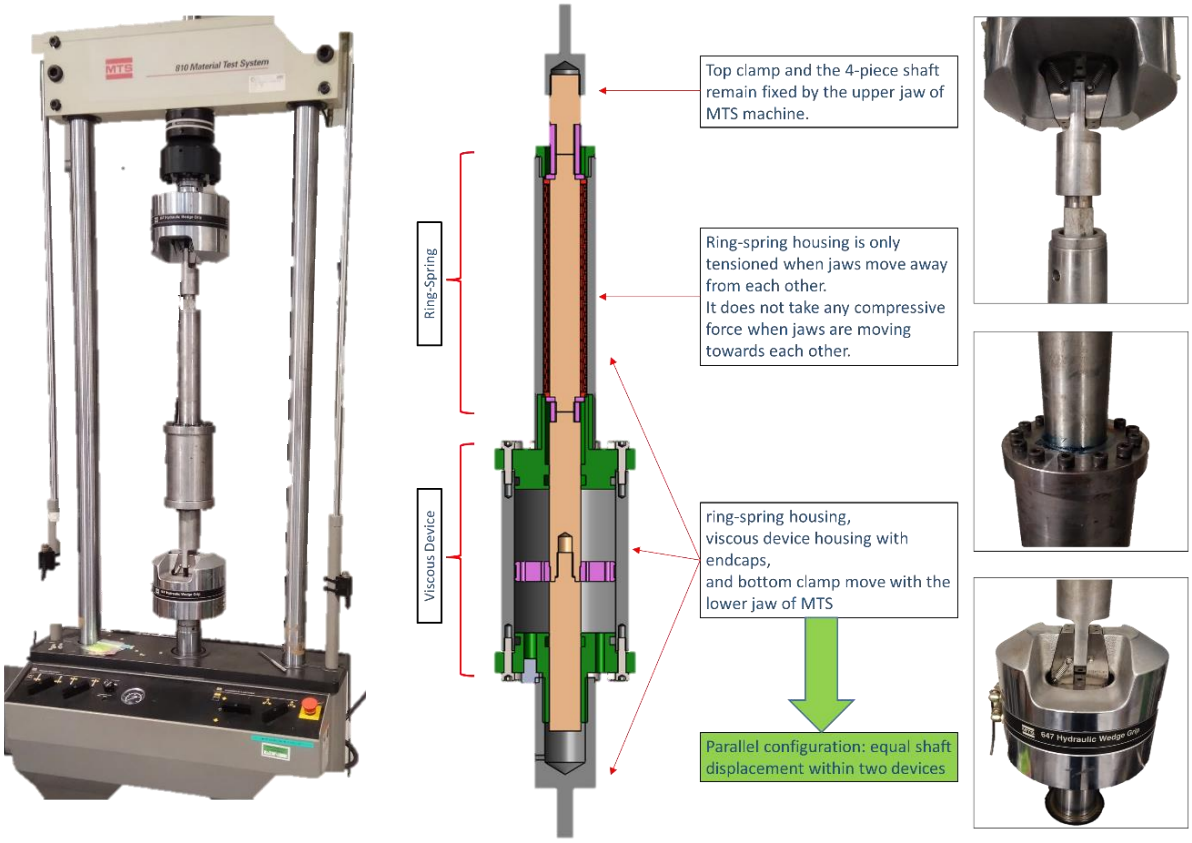


*Figure 15: Hybrid device setup and configuration in an MTS-810 hydraulic test machine*

# Lead Extrusion and Ring Spring Hybrid Device

In addition to the hybrid device that combines the viscous fluid damper with friction ring springs, a hybrid combination of a lead extrusion damper and ring springs was also designed and experimentally tested. This hybrid damping device combined the weakly velocity dependent lead extrusion damper with a re-centering ring spring, to enable a combined device where the initial and post-yield stiffness, as well as the nominal yield force can be independently varied. This ability to individually modify the yield point and post-yield stiffness can be used to define peak displacements in pushover analyses and to control the over-strength of a damper, which defines the design of the connecting elements.

The lead extrusion devices have been tested previously (Robinson and Greenbank, 1975, 1976) and exhibit a weakly velocity dependent elasto-plastic response behaviour. Depending on the relative force capacity of the lead extrusion and ring spring components, it is possibly to make minor changes to the post-yield stiffness (where most of the force comes from the lead extrusion device), or produce a completely self-centering hybrid device (where most of the force comes from the ring spring components). The best combination depends on the design requirements that are determined from the structural application.

## Lead Extrusion-Ring Spring Hybrid Device Design

An initial lead extrusion damper was designed to fit within an existing test rig. The lead extrusion damper was fitted within a brace that provided buckling restraint for compressive loading. An internal cavity was provided that allowed for the inclusion of friction ring springs to modify the post-yield stiffness. A cross-sectional view of the damper, with and without the inclusion of the ring springs, is presented in Figure 16. Similar to the viscous hybrid device, the ring spring components can only sustain compressive loading (or shortening of the stack from the original length). As such, the housing provided enables double-action. This configuration ensures that, regardless of the shaft motion, or whether the overall hybrid damper is undergoing compressive or tensile loading, the ring spring stack is always in compression.

Similarly to the viscous damper-ring spring hybrid damper, the overall configuration may initially look as though it is in a series configuration, but the design actually represents a parallel configuration. Both components undergo the same displacement (though there will be some disparity in displacement due to elastic axial flexure of the shaft) and the force contributions from each component add up to provide the resistive force produced by the hybrid device.

The lead extrusion component was designed for a design force of 450kN and the ring spring components had a design force at full compression of 65kN. This particular combination of parameters was intended to allow for the modification of the post-yield stiffness, rather than to create a fully self-centering hybrid damper.

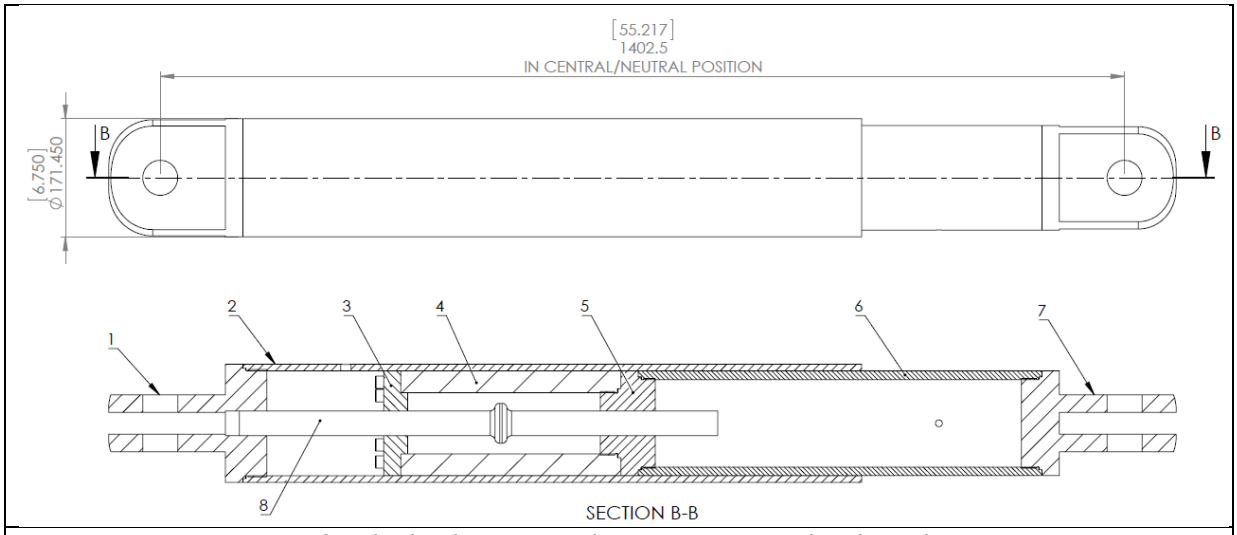


*a) The lead extrusion device incorporated within a brace*

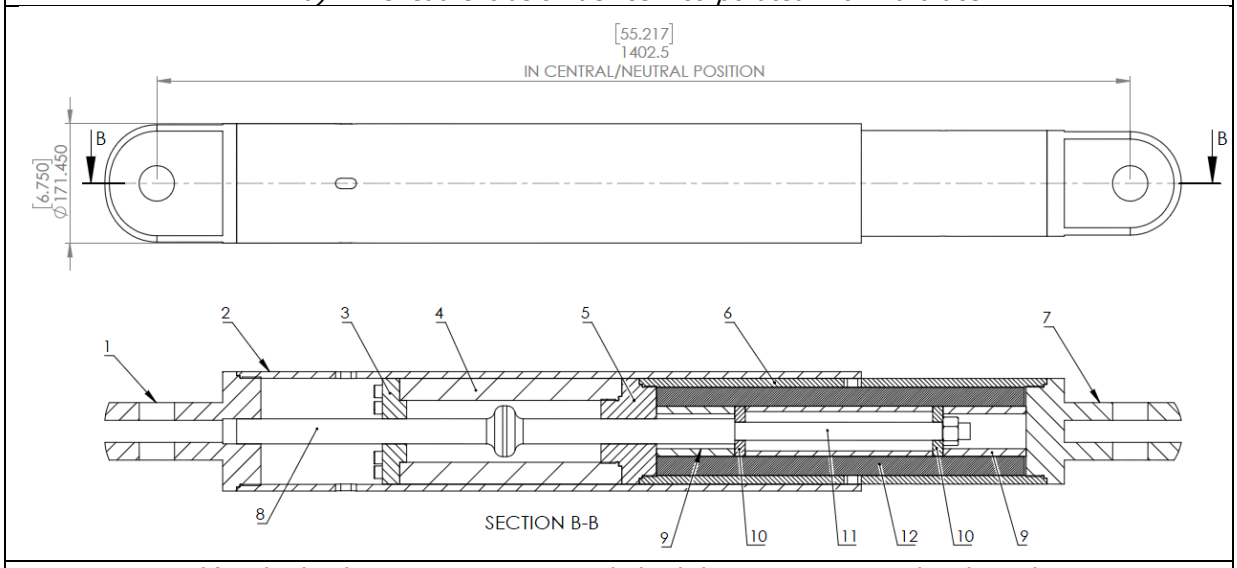


*b) The lead extrusion-ring spring hybrid device incorporated within a brace*

*Figure 16: Cross-section view of the lead-extrusion and ring-spring hybrid damper, with and without the inclusion of the spring components.*

# Experimental Setup and Methods

## Experimental Set-up – Lead Extrusion Hybrid Damper

The combined lead-extrusion and ring spring hybrid damper was mounted into a cyclic test configuration that represented the likely pin-end conditions that would be used for placement within a structure. This experimental set-up is shown in Figure 17. The test rig was capable of fully reversed cyclic loading at force up to 700kN, but did not have dynamic capability. Consequently, all testing undertaken to date on this hybrid device has been at quasi static load rates, with maximum velocity approximately 1 mm/s. While dynamic testing is desirable, this is the focus of ongoing research.

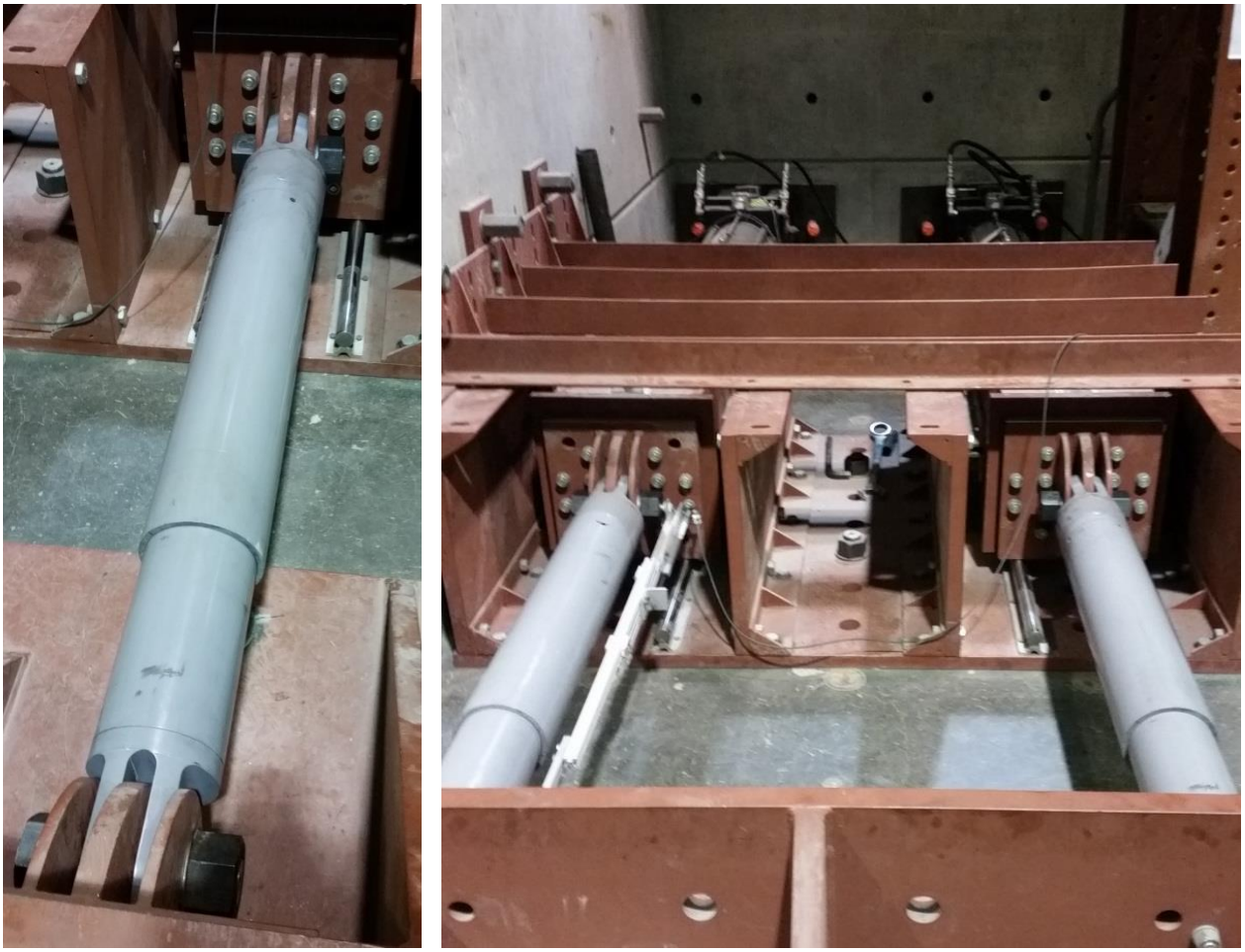

*Figure 17: Experimental set-up for the lead-extrusion and ring-spring hybrid damper specimens*

## Experimental Set-up – Self-Centering Viscous Damper

Experimental testing on the prototype hybrid device was carried out on an MTS-810 machine. The machine has lower and upper jaws with hydraulic wedge grips to hold the test device. The machine can initially be adjusted for the length of the device. The top jaw grips the top device clamp and remains fixed during the test, and the lower jaw transfers input displacement to the bottom device clamp creating the relative displacement between the two ends of the device as shown previously in Figure 15. Force and displacement sensors are located under the lower jaw to record the ram input displacement and reaction force.

This MTS-810 test machine has a force capacity of 100 kN and saturation input velocity of ~330 mm/s. The data acquisition system recorded force and displacement of the lower ram/jaw at a frequency of 1000 Hz.

## Input Displacement Profiles - Self-Centering Viscous Damper

A series of input displacements and frequencies were used to get comprehensive force displacement graphs, and to determine damping coefficients for the viscous device.

Table 6 lists the input values used in the experiments where there are 6 sets of 4-5 tests with approximately equal peak velocity. This format ensures that there are enough data points to calculate damping characteristics. Each test consisted of 3 complete cycles and after every 5 tests, the device was rested to allow the oil to cool, so built-up heat did not impact the fluid viscosity damping characteristics.

*Table 6: Input parameters for the viscous device tests*

| Stroke (mm) | Frequency (Hz) | Peak velocity (mm/s) | Stroke (mm) | Frequency (Hz) | Peak velocity (mm/s) |
|---|---|---|---|---|---|
| S = 10 | f = 0.80 | V = 50.24 | S = 10 | f = 3.20 | V = 200.96 |
| S = 20 | f = 0.40 | V = 50.24 | S = 20 | f = 1.60 | V = 200.96 |
| S = 30 | f = 0.27 | V = 50.87 | S = 30 | f = 0.07 | V = 201.59 |
| S = 40 | f = 0.20 | V = 50.24 | S = 40 | f = 0.80 | V = 200.96 |
| S = 50 | f = 0.16 | V = 50.24 | S = 50 | f = 0.64 | V = 200.96 |
| S = 10 | f = 1.60 | V = 100.48 | S = 10 | f = 4.00 | V = 251.20 |
| S = 20 | f = 0.80 | V = 100.48 | S = 20 | f = 2.00 | V = 251.20 |
| S = 30 | f = 0.54 | V = 101.74 | S = 30 | f = 1.33 | V = 250.57 |
| S = 40 | f = 0.40 | V = 100.48 | S = 40 | f = 1.00 | V = 251.20 |
| S = 50 | f = 0.32 | V = 100.48 | S = 50 | f = 0.80 | V = 251.20 |
| S = 10 | f = 2.40 | V = 150.72 | S = 10 | f = 4.80 | V = 301.44 |
| S = 20 | f = 1.20 | V = 150.72 | S = 20 | f = 2.40 | V = 301.44 |
| S = 30 | f = 0.80 | V = 150.72 | S = 30 | f = 1.60 | V = 301.44 |
| S = 40 | f = 0.60 | V = 150.72 | S = 40 | f = 1.20 | V = 301.44 |
| S = 50 | f = 0.48 | V = 150.72 | *** | *** | *** |

The ring stack consisted of 20 outer rings and 19 inner rings giving it an allowable total stroke of 38 mm. A 5-50% level of preload is the recommended preload for these devices to ensure proper interaction of the mating surfaces (RINGFEDER, 2016). Two pre-compression levels were applied to the ring-spring using the combination of washers in Table 7.

*Table 7: preload and stroke values for the prototype ring-spring*

| Pre-displacement (mm) | Preload (%) | Available stroke (mm) |
|---|---|---|
| 0 | 0 | 38 |
| 2.6 | ~7 | 35.4 |
| **8** | **~21** | **30** |
| **13** | **~34** | **25** |

Test results are presented as force-displacement graphs. The linear relation between force and velocity for the viscous device, and velocity saturation of the MTS machine, is shown using peak force-velocity graphs. Results can be compared to design values and expected behaviour.

# Results and Discussion

The following sections include the test results of the individual viscous damper, ring-spring damper, and the hybrid device respectively.

## Individual Component Tests - Viscous Fluid Damper

Figure 18 (left) shows a one-to-one comparison of the commanded input velocities and actual output (MTS jaw) velocities. While there is an accurate correlation for lower velocities, the MTS machine is not capable of faithfully carrying out input command velocities for desired velocities higher than ~330 mm/s. This value defines its saturation velocity.

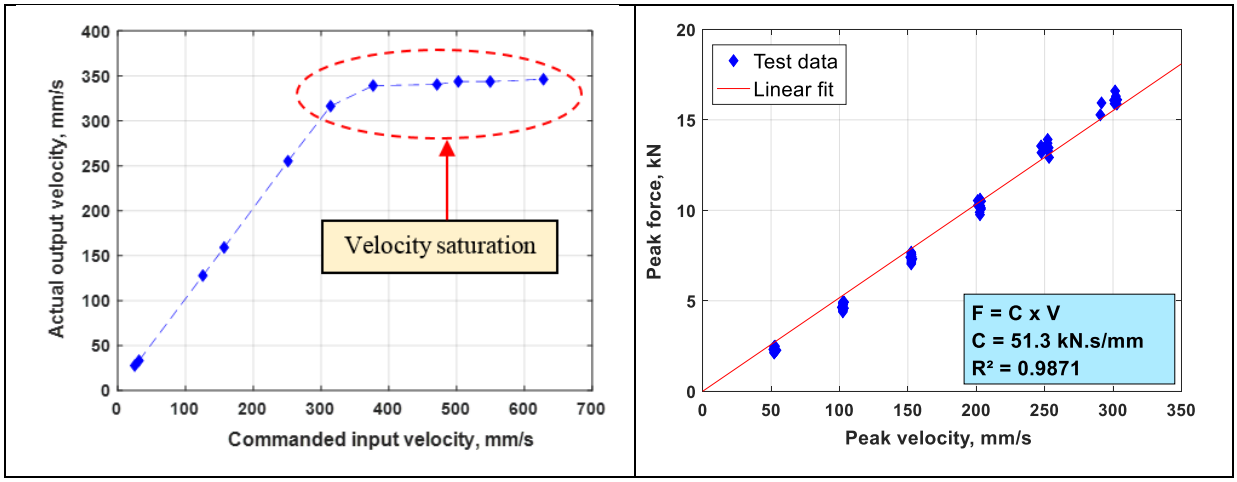


*Figure 18: Saturation of output velocity in the MTS machine (left) and linear regression of force-velocity correlation for the viscous device (right)*

Figure 18 (right) shows the damping force of the viscous device for velocities of V = [50 100 150 200 250 300] mm/s. There is a strong linear relation between device force and relative input velocity as expected. Linear regression gives the equivalent linear viscous damping coefficient for the viscous device with the current configuration of the open orifices as 51.3 kN.s/mm.

Figure 19 shows the force-displacement graphs for 2 of the input stroke levels (s = 25, 30 mm) and input frequency range of f = [0.25 – 1.75] Hz. The stroke levels are chosen similar to those of the ring-spring damper to enable easy comparison between the two devices. The maximum force level increases as the input velocity is increased due to the linear force-velocity relationship. For relatively small frequencies, the viscous forces should approach zero. However, the forces associated with the friction between piston and housing and between the shaft and seals exert a small but finite force on the shaft as seen in the graph for f = 0.25 Hz. Overall, the force-displacement graphs of the viscous device show an elliptic form, which agrees with expectations and previous findings of such dissipative devices (Hazaveh et al., 2016).

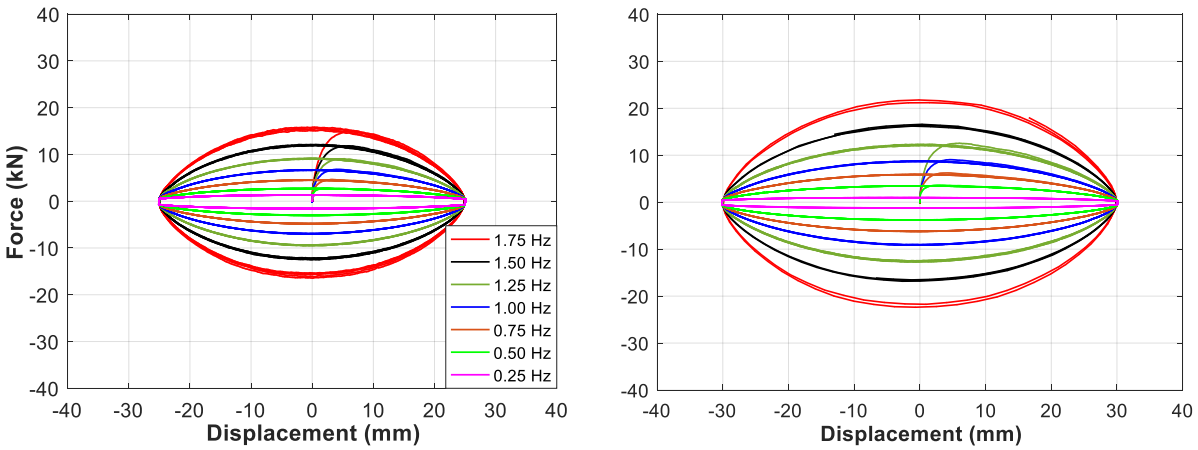


*Figure 19: Force displacement graphs for the viscous device with different input frequencies, stroke = 25 mm (left), and stroke = 30 mm (right)*

## Individual Component Tests on the Ring Springs

Figure 20 shows the force-displacement graph for ring-spring with pre-load levels in Table 7. As the preload is increased, the maximum allowable stroke of the device is lowered by the same amount. The ring-spring with 21% preload needs a compressive force of ~2kN before undergoing significant deformation. For 34% preload, this force is ~8kN. Several tests with different frequencies but equal strokes produced identical results validating the velocity-independent behaviour of the ring-spring as shown in Figure 21. As expected, the peak device forces occurred at peak displacement.

In addition, the return ratio of ring-spring defined as the ratio of unloading stiffness to loading stiffness, was seen to be 34% for this type of rings and grease where the loading stiffness is 0.6 kN/mm and the unloading stiffness is 0.2 kN/mm.

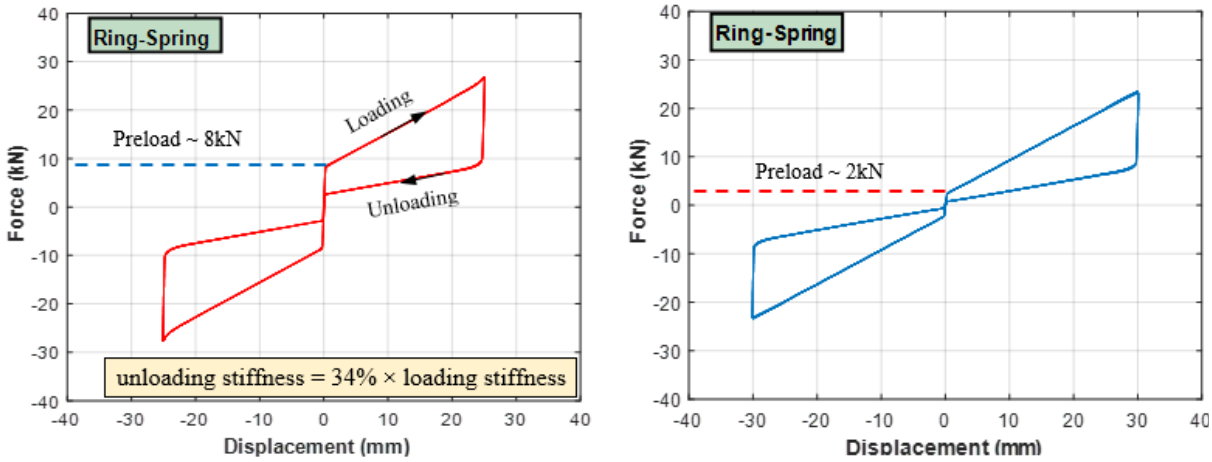


*Figure 20: Force displacement graphs for the ring-spring damper, preload = 34%, stroke = 25 mm (left), and preload = 21%, stroke = 30 mm (right)*

The ring-spring is also tested for the overloaded case. Figure 21 shows the force-displacement response of the ring-spring slightly beyond its nominal design capacity. In this case, the stack will display highly rigid behaviour, protecting the rings against excessive peripheral/circumferential stresses

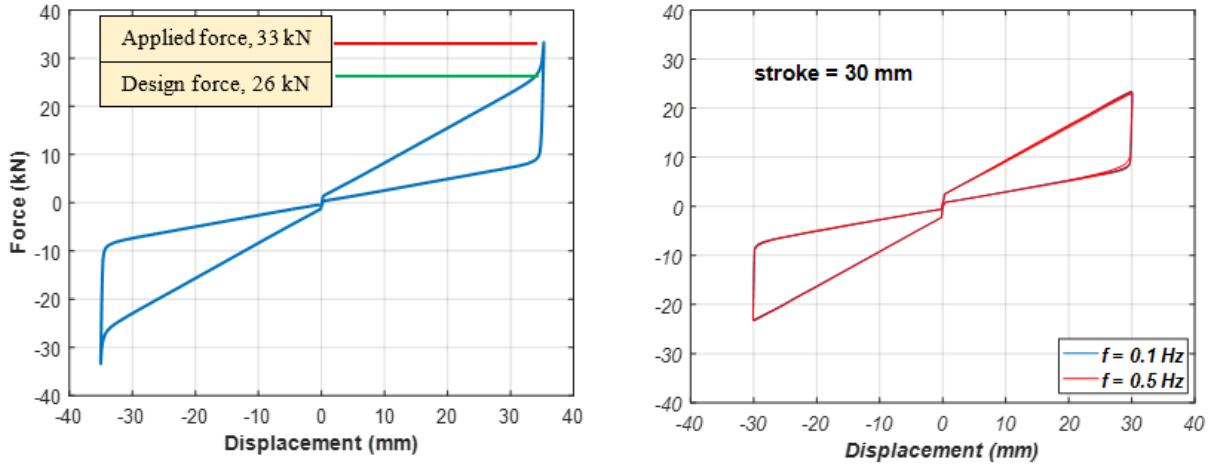


*Figure 21: Force displacement for overloaded ring-spring (left) and velocity independence of ring-spring response (right)*

## Hybrid Device Results - Self-Centering Viscous Damper

Figure 22 shows force-displacement graphs of the hybrid device under cyclic testing. The combination of two device behaviours creates a unique hysteretic loop. For lower frequencies, the graphs looks similar to that of the ring-spring alone as the force contribution of the viscous device is minimised at low velocities. However, the friction force from the viscous device is still present. As the input velocity (frequency) increases, the viscous action impacts the shape and the overall resistive force. For higher frequencies, the point of peak force moves from maximum displacement (zero velocity) towards zero displacement (maximum velocity). Moreover, the value of peak force is greater than the individual peak forces coming from the individual components devices for the same set of input displacements.

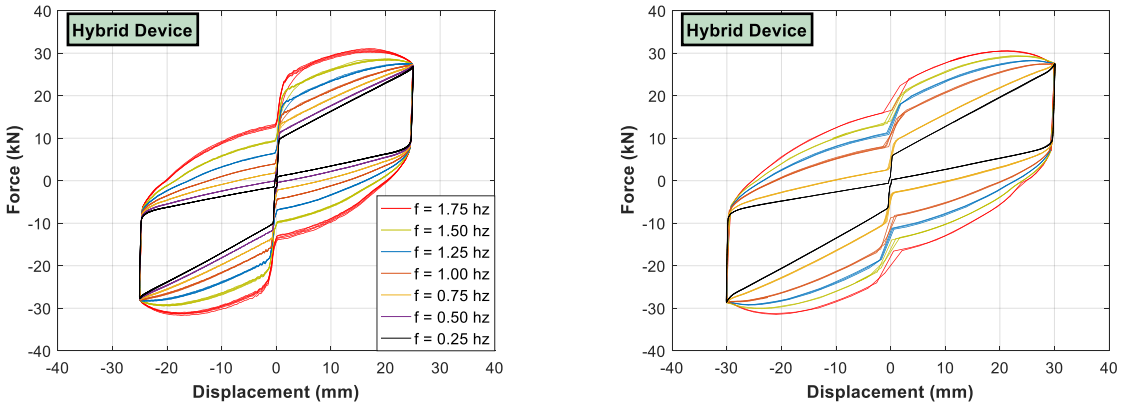


*Figure 22: Force displacement graphs for the hybrid device, RS preload = 34%, stroke = 25 mm (left), and RS preload = 21%, stroke = 30 mm (right)*

The hysteretic force displacement graphs of the hybrid device (Figure 22) show the combination of the two individual dissipaters (Figures 19 and 20). The combination of velocity independent behaviour (ring-spring) and velocity dependent (viscous damper) offers a measure of robustness in structural response to ground motions of different types (near-fault and far-fault) and their velocity content.

## Hybrid Device Results – Lead Extrusion Ring Spring Damper

The lead extrusion device alone and the combined lead-extrusion and ring-spring damper was subjected to a two fully reversed cycles at 40mm input displacement amplitude and 0.5 mm/s load rate. The results for the two configurations are presented in Figure 23. The lead extrusion device alone exhibited an essentially elastic perfectly-plastic response behaviour with almost no post-yield stiffness. Conversely, the combined hybrid device, with the inclusion of the ring springs exhibits a non-zero post-yield stiffness, as intended by design. By tailoring the spring design force and design stroke capacity, the post-yield stiffness can be modified independently of the overall level of resistive force.

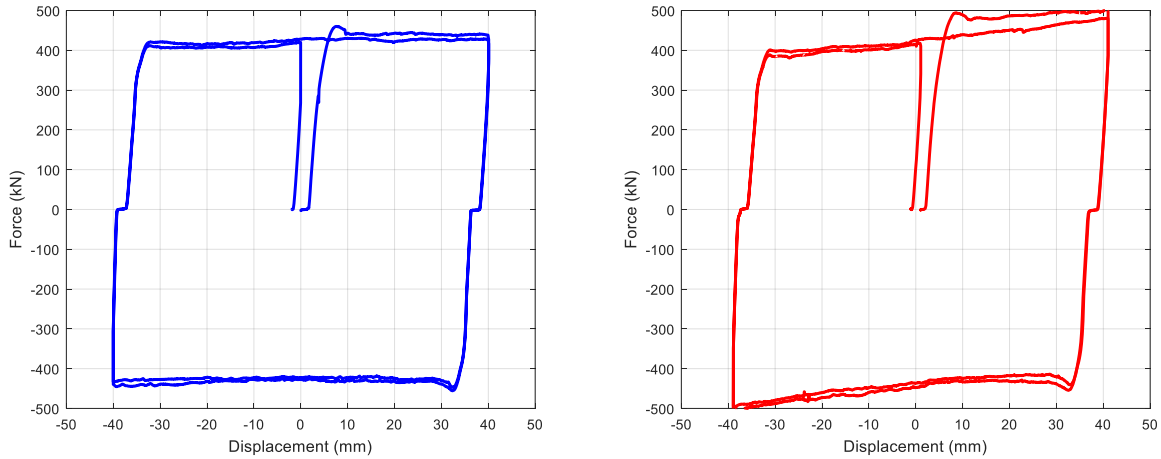


*Figure 23: Cyclic test results for the lead extrusion device alone (left) and the hybrid lead-extrusion and ring-spring damper (right). The presence of the ring spring components has modified the post-yield stiffness of the hybrid device.*

# Conclusions and Recommendations

Comprehensive testing of a prototype hybrid dissipation device and its individual components across a range of input strokes and frequencies was done in this research. The hybrid device consists of a viscous fluid damper and friction-based rings-springs. Based on the experimental procedure and results, the following conclusive remarks could be stated:

The hybrid device consists of a viscous damper and a friction ring-spring thus, combining velocity-dependent and velocity independent characteristics of the two components.

- The viscous device shows consistent dissipative behaviour with a linear correlation between the force and input velocity
- The ring-spring shows a consistent velocity independent, flag-shaped behaviour offering re-centring with a level of dissipation
- The maximum allowable displacement depends on the nominal length (number of rings) and the adjusted preload
- The hybrid device shows a hysteretic behaviour combining the highly dissipative behaviour of the viscous device and the re-centring characteristics of the ring-spring

Overall, the use of a combination of damping device components, whether integrated into a single hybrid device, as presented within this study, or incorporated as separate devices into a single structural system, allows a designer to tailor individual aspects of the structural damping behaviour. Initial and post-yield stiffness, nominal 'yield' force and the velocity dependence of the damping system can all be individually modified to produce an overall structural response that meets design targets.

# References


AISC 2005. Seismic provisions for structural steel buildings. Chicago, Illinois, American Institute of Steel Construction.

Anderson, J., Gourley, B., Green, M., Hajjar, J., Johnston, R., Leon, R., Sullivan, D. and Partridge, J. 1995. Case studies of steel moment frame building performance in the Northridge earthquake of January 17, 1994. Report no. SAC, 95(07).

Barroso, L.R., Chase, J.G. and Hunt, S. 2003. Resettable smart dampers for multi-level seismic hazard mitigation of steel moment frames. Journal of Structural Control, 10(1): 41-58.

Buckle, I. (1994). The Northridge, California earthquake of January 11, 1994: performance of highway bridges, Tech. Rep. NCEER-94-0068, National Center for Earthquake Engineering Research.

Constantinou, M.C. and Symans, M. 1992. Experimental and analytical investigation of seismic response of structures with supplemental fluid viscous dampers, National Center for earthquake engineering research Buffalo, NY.

Emilio, R. and Roberto, M. 1986. The 1985 Mexico Earthquake. Concrete International, 8(5).

Erasmus, L. 1988. Ring springs on holding-down bolts for seismic energy dissipation. Transactions of the Institution of Professional Engineers New Zealand: Civil Engineering Section, 15(2): 41-47.

Fahnestock, L.A., Sause, R. and Ricles, J.M. 2007. Seismic Response and Performance of Buckling-Restrained Braced Frames. Journal of Structural Engineering, 133(9): 1195-1204.

Djojo, G.S., Clifton, G.C., Henry, R. and Macrae, G. 2017. Experimental validation of Rocking CBFs with Double Acting Ring Springs. pp.1-8. New Zealand Society of Earthquake Engineeering Annual Conference Wellington, New Zealand.

Hazaveh, N.K., Pampanin, S., Rodgers, G. and Chase, J. 2016. Design and experimental test of a Direction Dependent Dissipation (D3) device with off-diagonal (2-4) damping behaviour. pp.1-7. Proceedings of the New Zealand Society for Earthquake Engineering (NZSEE) Annual Technical Conference, Christchurch, New Zeland.

Hill, K.E. (1995). The Utility of Ring Springs in Seismic Isolation Systems: A Thesis Submitted for the Degree of Doctor of Philosophy University of Canterbury.

Holzer, T.L. and Savage, J.C. 2013. Global earthquake fatalities and population. Earthquake Spectra, 29(1): 155-175.

Ibrahim, R.A. 2008. Recent advances in nonlinear passive vibration isolators. Journal of Sound and Vibration, 314(3-5): 371-452.

Mageba (2013). Seismic protection devices for reliable preservation of structures, Preloaded Spring Damper. Mageba. Switzerland: 1-4.

Mander, J.B. and Cheng, C.-T. (1997). Seismic resistance of bridge piers based on damage avoidance design, National Center for Earthquake Engineering Research.

Mimura, N., Yasuhara, K., Kawagoe, S., Yokoki, H. and Kazama, S. 2011. Damage from the Great East Japan Earthquake and Tsunami - A quick report. Mitigation and Adaptation Strategies for Global Change, 16(7): 803-818.

Priestley, M.N., Sritharan, S., Conley, J.R. and Pampanin, S. 1999. Preliminary results and conclusions from the PRESSS five-story precast concrete test building. PCI journal, 44(6): 42-67.

Ringfeder (2016). Damping Technology. Germany, RINGFEDER GmbH.

Robinson, W. H., and Greenbank, L. R. (1975). "Properties Of An Extrusion Energy Absorber." Bulletin of the New Zealand Society for Earthquake Engineering, 8(3),187-191.

Robinson, W. H., and Greenbank, L. R. (1976). "Extrusion Energy Absorber Suitable For The Protection Of Structures During An Earthquake." Earthquake Engineering & Structural Dynamics, 4(3), 251-259.

Rodgers, G.W., Solberg, K.M., Chase, J.G., Mander, J.B., Bradley, B.A., Dhakal, R.P. and Li, L. 2008. Performance of a damage-protected beam-column subassembly utilizing external HF2V energy dissipation devices. Earthquake Engineering & Structural Dynamics, 37(13): 1549-1564.

Sabelli, R., Mahin, S. and Chang, C. 2003. Seismic demands on steel braced frame buildings with buckling-restrained braces. Engineering Structures, 25(5): 655-666.

Solberg, K., Mashiko, N., Mander, J. and Dhakal, R. 2009. Performance of a damage-protected highway bridge pier subjected to bidirectional earthquake attack. Journal of structural engineering, 135(5): 469-478.

Solberg, K.M. 2007. Experimental and financial investigations into the further development of damage avoidance design.

Soong, T.T. and Spencer, B.F. 2002. Supplemental energy dissipation: state-of-the-art and state-of-the-practice. Engineering Structures, 24(3): 243-259.

Symans, M.D., Charney, F.A., Whittaker, A.S., Constantinou, M.C., Kircher, C.A., Johnson, M.W. and Mcnamara, R.J. 2008. Energy dissipation systems for seismic applications: Current practice and recent developments. Journal of Structural Engineering, 134(1): 3-21.

Treasury, N.Z. (2014). 2014 Budget: Budget Policy Statement. Wellington, New Zealand.

# Structural Modelling of Damping Devices

## Executive Summary

The viscous dampers, ring springs, and the combined hybrid device have been well proven through the experiment test programme presented in the previous section. Each individual component exhibits a highly repeatable and predictable response profile, which makes modelling of a range of possible damping device configurations easy and reliable. From the results presented in the previous section, it would be easy to produce a hybrid damping device with a specific target performance, where the ring spring parameters (preload, loading stiffness, unloading stiffness, design force and displacement capacity) can be individually tailored to achieve an optimum overall structural response. Likewise, the viscous fluid damping component can be modified to alter the damping characteristics that it contributes to the overall hybrid device.

The multitude of design parameters available to tailor the characteristics of an overall hybrid damping device presents a significant opportunity to produce a damping device with a specific response behaviour. However, it may be difficult to determine how the damping device design parameters affect the overall response of a structure. This research seeks to undertake seismic response modelling with a range of different structures, to ascertain the influence of different device design parameters on structural response. Results are presented as reduction factors, so that easy comparisons can be made between different responses.

## Structural Modelling – Lead Extrusion and Ring Spring Hybrid

### Analysis Summary

This research investigates the structure-level influence of the use of hybrid damping devices consisting of ring springs and lead extrusion dampers. Dynamic behaviour of a system with nonlinear structural stiffness and supplemental hybrid damping via lead extrusion devices and ring spring dampers is used to investigate the design space and potential. Lead extrusion devices are modelled with design forces equal to 5% and 10% of seismic weight and ring springs are modelled with loading stiffness values of 20% and 40% of initial structural stiffness and respective unloading stiffness of 7% and 14% of structural stiffness (equivalent to 35% of their loading stiffness). Using a suite of 20 design level earthquake ground motions, nonlinear response spectra for 8 different configurations are generated. Results show up to 50% reduction in peak displacements and greater than 80% reduction in residual displacements of augmented structure compared to the baseline structure. These gains come at a cost of a significant rise in the base shear values up to 200% mainly as a result of the force contributed by the supplemental devices.

## Analysis Parameters and Model

The lead extrusion device behaviour may be modelled using a velocity-dependent nonlinear relation (Rodgers et al., 2008):

$$F_D = C_\alpha |\dot{y}|^\alpha \tag{8}$$

where $F_D$ is the damper force, $\alpha$ is the velocity exponent, which is within the range of [0.11-0.15], $C_\alpha$ is the geometry dependent damper constant, and $\dot{y}$ is the shaft velocity.

Minimizing possible damage and/or repair costs is a common goal of structural design. To this end, determining maximum level of key response metrics including peak and residual displacement and peak base shear need to be thoroughly investigated and predicted. Minimizing peak structural displacement can reduce the deformation of individual structural components decreasing associated damage (Chiou *et al.*, 2011; Ruiz-García and Aguilar, 2015). Residual displacements are associated with post-event repair costs (Bazzurro *et al.*, 2004; Luco *et al.*, 2004; Polese *et al.*, 2013; Salari and Asgarian, 2015), but are often neglected in the design process. Finally, overall column force and total base shear force is directly related to required column strength and foundation demands (Elnashai *et al.*, 2004).

This research investigates the influence of using a supplemental hybrid High Force-to-Volume (HF2V) plus ring spring damping device on the structural response parameters of a nonlinear structure. The structure has an elasto-plastic hysteretic behaviour thus exhibiting typical inelastic structural behaviour. The proposed hybrid device incorporates lead extrusion devices for their force capacity and dissipation and ring springs to add recentring. Nonlinear spectral analysis is done for a variety of HF2V and ring spring device capacities to parametrise their potential across a reasonable device design space.

A typical single-degree-of-freedom (SDOF) system for spectral analysis is shown in Figure 24. Such models are regularly used in spectral analyses upon which performance based design codes rely (Chopra and Goel, 2001; Subramanian and Velayutham, 2014). In this case, the system includes a nonlinear elasto-plastic hysteresis for the structure and a supplemental damping system that is a hybrid of nonlinear HF2V and ring spring devices. The nonlinear structure is subjected to horizontal unidirectional seismic acceleration, $\ddot{z}_g$ with and without supplemental devices.

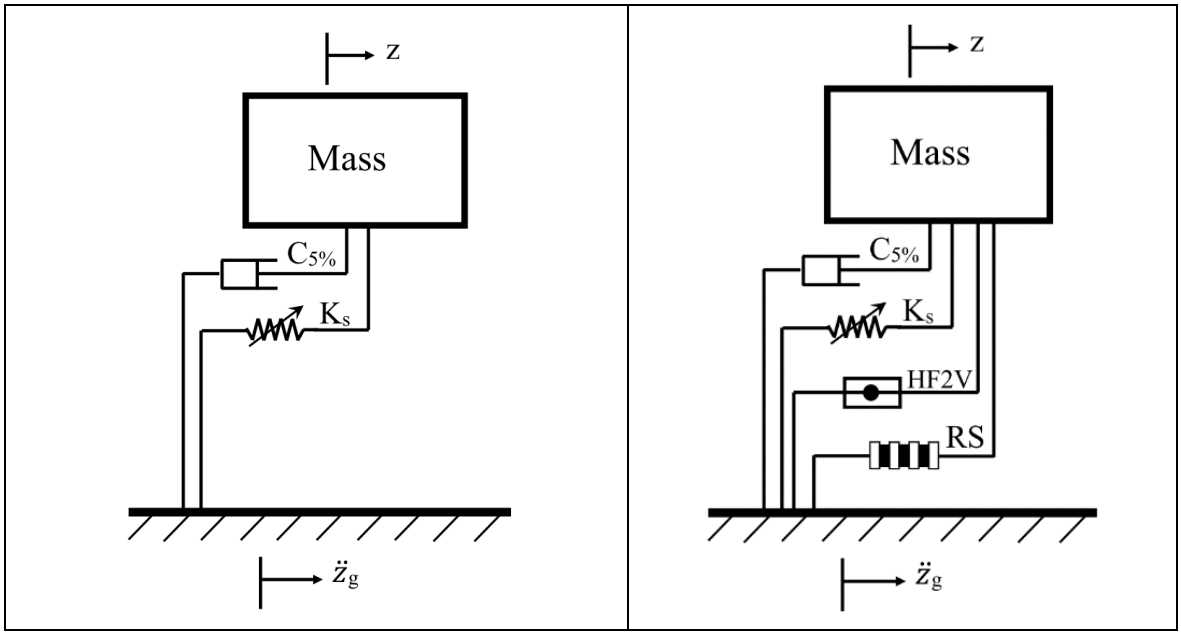


*Figure 24: Schematic configuration of a SDOF system and ground motion input. Left: uncontrolled baseline structure; Right: controlled/augmented struture (with supplemental devices)*

## Nonlinear Structure Model

In the previous sections, component tests of the damping devices have been undertaken and structural-level modelling has been completed to determine the likely response of a structure fitted with this type of supplemental damping system. Finally, to combine these aspects, the devices developed were included in a 14-tonne two-storey, low-damage steel frame structure that underwent testing on the University of Auckland shake table test facility. This important final step in the research combines the key theme of the previous two sections, to determine if the predicted response behaviour at the structural-level matches the predictions made from the computational study.

Nonlinear elasto-plastic restoring force is modelled using the Menegotto-Pinto model (Menegotto and Pinto, 1973):

$$F = \rho kz + \frac{(1-\rho)kz}{\left[1+\left|kz/F_Y\right|^{\beta}\right]^{1/\beta}} \tag{9}$$

where $F$ is the structural force, $z$ is the deformation, $F_Y$ is the yield force, and $k$ is the stiffness. The parameters $\rho$ and $\beta$ are used to define the shape of the curve, where $\rho$ is the ratio of post-yield stiffness to pre-yield stiffness and β determines the shape of the transition curve.

## Lead Extrusion Device Model

The lead extrusion damper may be mathematically modelled using the Maxwell type mass-spring configuration (Rodgers *et al.*, 2012). The total shaft displacement, *z*, is the sum of two separate components; linear elastic elongation of the device shaft, *x*, and the nonlinear bulge displacement within the cylinder, *y*, as in Figure 25 yielding:

$$x + y = z \tag{10}$$

Due to the series nature of the spring-damper model, the spring (representing the elastic deflection of the shaft) and damper have an equivalent force. Experimental results (Cousins *et al.*, 1991; Rodgers *et al.*, 2008) indicate this force is related to the shaft velocity:

$$F_D = C_\alpha \left|\dot{y}\right|^\alpha = \frac{x}{f_D} \tag{11}$$

where $\alpha$ is the velocity exponent, $C_\alpha$ is the geometry dependent damper constant, and $f_D$ is the spring flexibility. Combining Eqs. (10) and (11) yields:

$$\left(\frac{F_D}{C_\alpha}\right)^{1/\alpha} = \dot{z} - f_D \dot{F}_D \tag{12}$$

Converting Eq. (12) to the finite difference form and rearranging the terms yields:

$$\Delta t \left(\frac{F_{D,i+1}}{C_\alpha}\right)^{1/\alpha} + f_D F_{D,i+1} = z_{i+1} - z_i + f_D F_{D,i} \tag{13}$$

where *i* is the time index. Note that the right hand side of the equation consists of known parameters at each time step, $t_i$. To find $F_D$ from Eq. (13), an iterative method is required. Thus, the equation is rewritten:

$$F_{D,i+1} = C_\alpha \left(\frac{z_{i+1} - z_i + f_D F_{D,i}}{\Delta t + C_\alpha f_D F_{D,i+1}^{\,1-1/\alpha}}\right)^\alpha \tag{14}$$

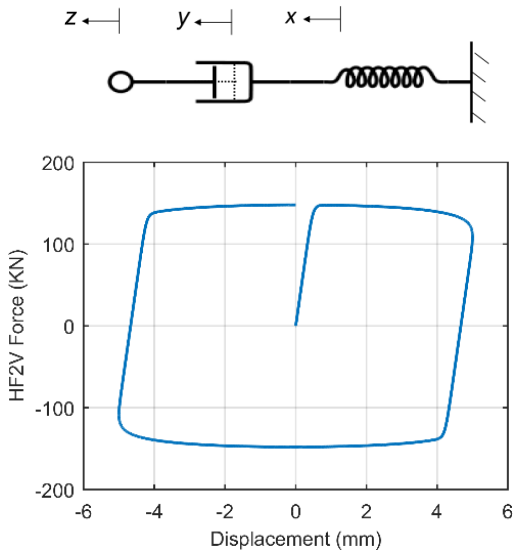


*Figure 25: Schematic configuration (top) and force-displacement behavior of a HF2V device (bottom)*

Comparing Eq. (14) and Eq. (11), the bracketed term is indeed the shaft velocity at instance $t_{i+1}$. To avoid erroneous results due to the fractional exponent and also considering the direction of motion, Eq. (14) is broken into two separate parts:

$$\dot{y}_{i+1} = \frac{z_{i+1} - z_i + f_D F_{D,i}}{\Delta t + C_\alpha f_D F_{D,i+1}^{1-1/\alpha}} \tag{15}$$

$$F_{D,i+1} = C_\alpha \left|\dot{y}_{i+1}\right|^\alpha \times sign\left(\dot{y}_{i+1}\right) \tag{16}$$

Using sufficiently small time increments and a sufficient number of iterations in each step, Eqs. (15)-(16) will yield $F_D$. The resulting force-displacement behaviour shown in Figure 25 (Rodgers *et al.*, 2011) is in agreement with finite elements results of Yang *et al.*, (2015).

## Ring Spring Model

To model the behaviour of a stacked ring spring, a single ring is isolated to show the forces acting on an inner ring, as shown in Figure 26. Since the direction of the friction force depends on the direction of axial motion, the relation between the axial force and axial displacement of the ring, which represents the axial stiffness, will be different depending on whether the rings are moving apart (unloading) or the gap between them is closing (loading). It can be proved that the ratio of the increasing axial stiffness to the decreasing axial stiffness is defined (Erasmus, 1988):

$$\frac{K_d}{K_i} = \frac{(\mu - \tan(\alpha))(1 - \mu\tan(\alpha))}{(1 + \mu\tan(\alpha))(\mu + \tan(\alpha))} \tag{17}$$

where $K_d$ is the decreasing (unloading) stiffness and $K_i$ is the increasing (loading) stiffness. Figure 26 also shows the typical behaviour of a ring spring in terms of force-displacement diagram.

As expected, increasing stiffness is always greater than the decreasing stiffness. However, the stiffness and the total displacement capacity of the ring spring may be manipulated by using a different number of rings in a stack, using different configurations (parallel or series) of ring springs, and utilising different lubricants to lower the frictional coefficient (Hill, 1995). As evident in Figure 26, the displacement corresponding to zero force is zero. This result ensures self-centring, which is an important characteristic of these devices and proves useful in managing nonlinear seismic displacements.

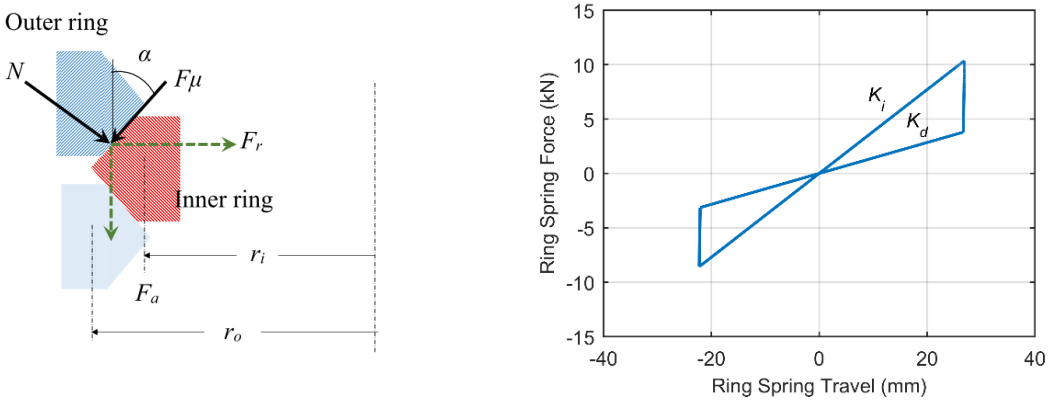


*Figure 26: Resolved forces on the inner ring (left) and force-displacement behavior of a ring spring device (right)*

## Hybrid Device Model

Combining the high dissipation of a HF2V device and the recentring ability of a ring spring, may provide benefits over using each component alone. However, the nonlinear nature of these devices precludes a direct formulation to predict their behaviour in a structure. While the nonlinearity of ring spring dynamics is the result of its direction-dependent multi-value stiffness, the nonlinearity of HF2V is because of its velocity-dependent force. The combination of such behaviours makes the design process more complicated.

Eq. (18) shows the governing equation of motion for the system shown in Figure 24 including this hybrid device:

$$m_e\ddot{z} + c\dot{z} + F_{NL} + F_{RS} + F_{HF2V} = -m_e\ddot{z}_g \tag{18}$$

where $m_e$ is the seismic mass of the structure, $F_{NL}$ is the nonlinear structural restoring force, $F_{RS}$ is the ring spring force, and $F_{HF2V}$ is the lead-extrusion damper force.

The impact of each component on the overall behaviour of the hybrid device depends on their design parameters. The HF2V contribution is defined by $\varepsilon$, which is defined as the ratio of peak HF2V force $C_\alpha$ in Eq. (11) to the seismic weight, $m_e g$ at a reference velocity of *1.0 m/s,* giving:

$$C_\alpha = \varepsilon m_e g \tag{19}$$

Moreover, the value $\alpha=0.12$ is used in Eq. (11) based on the experimental results (Cousins and Porritt, 1993; Rodgers *et al.*, 2006; Rodgers *et al.*, 2007). The ring spring force can be specified by its loading and unloading stiffness values ($K_i$ and $K_d$). A convenient way is to specify them as a percentage of pre-yield structural stiffness, $K_s$.

## Detailed Analysis Methodology

To investigate the impact of hybrid devices over a design space of non-dimensional damper capacity, $\varepsilon$ and $K_i / K_s$ , a nonlinear spectral analysis (Ewing *et al.*, 2009; Maniyar *et al.*, 2009) is conducted using the medium suite of design level earthquakes (shown in Table 8) from the SAC project (Somerville and Venture, 1997). This suite includes 20 acceleration time histories with a probability of exceedance of 10% in 50 years. The results can then be used to assess the reductions in structural response, base shear demand, and residual displacement, parametrised by the device design parameters $\varepsilon$ and $K_i / K_s$ over a full range of structural periods to ensure easy integration into performance based design.

*Table 8: Ground motion records used in the simulations (medium suite of records in SAC project)*

| No. | **SAC No.** | **Record name** | **PGA (g)** |
|---|---|---|---|
| **1** | (la01) | Imperial Valley, | 0.46 |
| **2** | (la02) | Imperial Valley, | 0.68 |
| **3** | (la03) | Imperial Valley, 1979, Array 5 | 0.39 |
| **4** | (la04) | Imperial Valley, 1979, Array 5 | 0.49 |
| **5** | (la05) | Imperial Valley, 1979, Array 6 | 0.30 |
| **6** | (la06) | Imperial Valley, 1979, Array 6 | 0.23 |
| **7** | (la07) | Landers Eqk, 1992 | 0.42 |
| **8** | (la08) | Landers Eqk, 1992 | 0.43 |
| **9** | (la09) | Landers Eqk, 1992 | 0.52 |
| **10** | (la10) | Landers Eqk, 1992 | 0.36 |
| **11** | (la11) | Loma Prieta, 1989, Gilroy | 0.67 |
| **12** | (la12) | Loma Prieta, 1989, Gilroy | 0.97 |
| **13** | (la13) | Northridge, 1994 | 0.68 |
| **14** | (la14) | Northridge, 1994 | 0.66 |
| **15** | (la15) | Northridge, 1994 | 0.53 |
| **16** | (la16) | Northridge, 1994 | 0.58 |
| **17** | (la17) | Northridge, 1994, Sylmar | 0.57 |
| **18** | (la18) | Northridge, 1994, Sylmar | 0.82 |
| **19** | (la19) | North Palm Springs, 1986 | 1.02 |
| **20** | (la20) | North Palm Springs, 1986 | 0.99 |

The model is presumed to have a nominal height, $H_e=10\ m$, a seismic mass, $m_e=10^4\ Kg$ with the pre-yield structural stiffness determined by the natural period of the uncontrolled structure, ($K_s=2\pi\ m_e^2/T$ ). A yield drift value of $\delta_y=2\%$ together with parameters $\rho=5\%$ and $\beta=20$ in Eq. (9) are used to model the nonlinear structural stiffness. To account for elastic dissipation losses, inherent structural damping equal to 5% of critical damping is considered. The nonlinear time history response of the structure is evaluated for the selected hybrid device configurations using the software package MATLAB. Peak response parameters including displacement and base shear are recorded together with the residual displacement at the end of oscillation.

The data extracted from the time history response of 20 earthquake records is used to evaluate the statistically representative metrics for each structural period. In accordance with the log-normal distribution of results, geometric mean values are used to show the average values of peak displacement and peak base shear, and median values are used for residual displacements. This process is repeated for structural periods in the range $T_n=[0.2\text{-}5]\ (s)$ with an increment $dT=0.1\ (s)$ to provide the response spectra (Maniyar *et al.*, 2009).

To better demonstrate how the supplemental damping alters the behaviour of a structure, the results are shown in the form of reduction factors. A reduction factor for a particular response metric is defined as a ratio of the modified structure response with added device to the uncontrolled structure response without device. As such, a value lower than *1.0* indicates a reduction in response (Bhunia *et al.*, 2012).

The response spectra are created for a set of parametrised hybrid device configurations. Two values of $\varepsilon=5\%$ and $\varepsilon=10\%$ are used to study the effect of HF2V capacity based on previous research (Rodgers *et al.*, 2008). Two different ring spring scenarios, $RS_{20}$ and $RS_{40}$, characterised by loading stiffness values of $K_i/K_s$ = 20% and $K_i/K_s$ = 40% are considered in the analyses, where $K_s$ is the pre-yield structural stiffness. For both ring springs, the unloading stiffness is considered to be 35% of the loading stiffness ($K_d/K_i$ = 35%), so $RS_{20}$ and $RS_{40}$ have the return stiffness ratio of 7% and 14% respectively.

The values of 5% and 10% storey weight for the HF2V device force capacity are defined from prior analyses done on steel beam-column connections (Rodgers et al., 2007). They are achievable device forces offering significant reductions and provide values below the equivalent plastic moment capacity of the beam depending on how it is specifically connected to the structure (Bacht et al., 2011). The ring springs are similarly scaled as a percentage of system stiffness to parametrise them to the structural design parameters. The values of 20% and 40% loading stiffness and respective return stiffnesses of 7% and 14%, as shown in Figure 26, are regarded in design as levels that enable recentring of structures (Khoo et al., 2012). Thus, these values were chosen based on the recentring stiffness they would offer as that was the primary reason for their use. However, a very wide range of possibilities is available, but these parameterised choices display the potential range of response achievable.

Each of the four components of $\varepsilon_5$, $\varepsilon_{10}$, $RS_{20}$, and $RS_{40}$ are utilized in the structural model separately and in combination to generate 8 hybrid device configurations with 3 spectral analysis plots ($RF_{disp}$, $RF_{shear}$, $RF_{res}$) for each configuration. The overall results should fully characterise the design specifications and relative impact of these devices. Such spectra can thus provide design input to performance based design methods.

# Analysis Results

## Displacement Results

The reduction factors (RFs) for displacement response are shown in Fig. 27. The HF2V device significantly decreases the peak displacement results (Fig. 27(a)) with an average 30% reduction for $\varepsilon_5$ and 45% reduction for $\varepsilon_{10}$ whereas only a 10-15% average reduction is seen for $RS_{20}$ and $RS_{40}$ (Fig. 27(b)). The combination of 5% HF2V and ring springs ($RS_{20}$, $RS_{40}$) results in the RFs shown in Fig. 27(c). An average value of 0.6 is obtained for the total period range with the difference between $RS_{20}$ and $RS_{40}$ being reasonably insignificant particularly for periods greater than 2 sec. Reduction factors for $\varepsilon_{10}$ and two ring springs show a similar trend to those of $\varepsilon_5$ (Fig. 27(d)), but with a further increase in displacement reductions ($RF_{disp}=0.5$). The relatively small difference between the results of the hybrid device with different ring spring sizes suggests that the use of larger ring springs would not be fully justified based on displacement reductions alone. Overall, HF2V devices provide the primary reductions in peak displacement, where Figure 27(a) results are in accordance with the linear spectral analyses of Rodgers *et al.*, (2008).

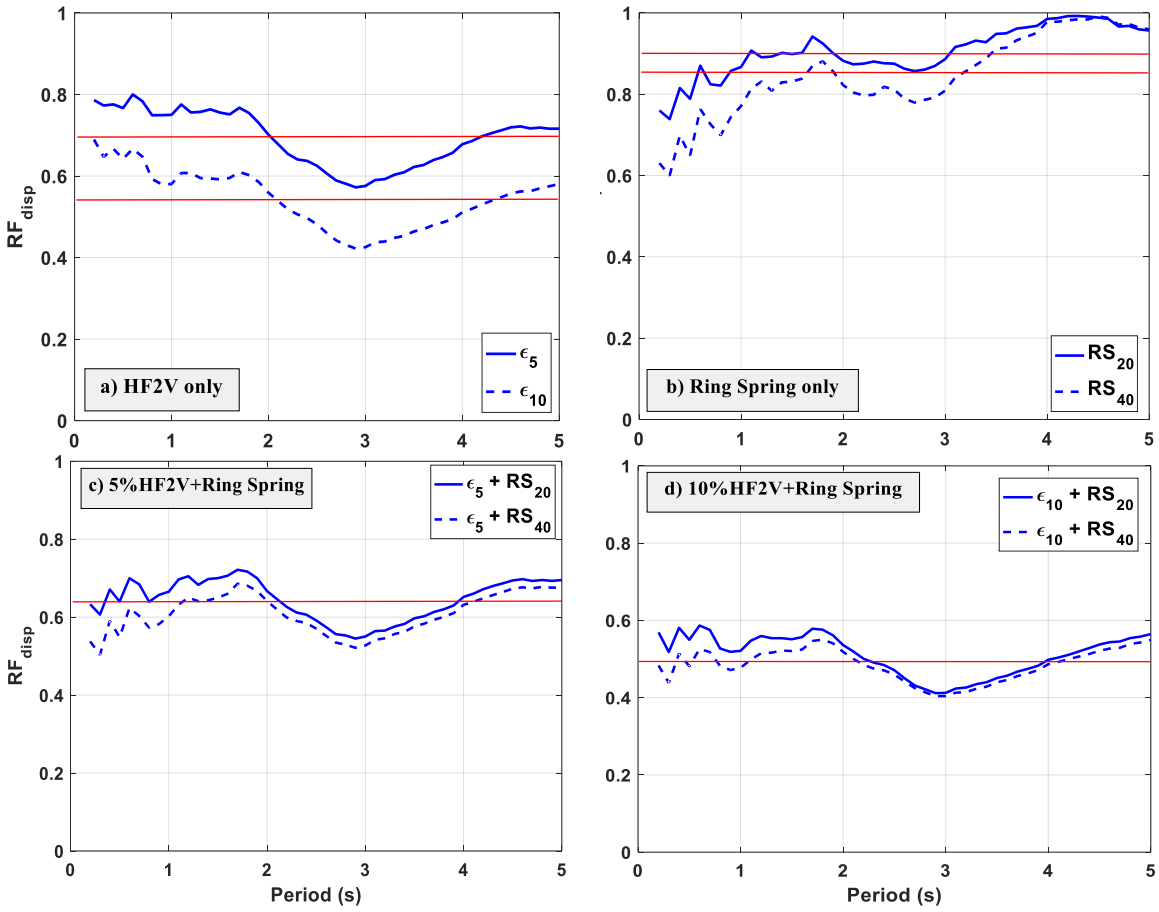


*Figure 27: Displacement RF results for: **a**) HF2V only; **b**) Ring Spring only; **c**) 5% HF2V with both ring springs; and **d**) 10% HF2V with both ring springs. Solid horizontal lines show average values for the results across all periods*

## Residual Displacement Results

Residual displacement RFs are shown in Fig. 28. Reduced residual displacements with only HF2V (Fig. 28(a)) are mainly due to the overall decreased displacements throughout the time history. However, the reductions resulted using only ring spring (Fig. 28(b)) are associated with recentring stiffness and the reduced displacement due to the damping from the ring springs. Hybrid devices, show markedly greater average reductions higher than 80%, combining the positive effects of HF2V and ring spring (Figs. 28(c)-(d)). If the residual displacement is important, then a larger ring spring is more favourable as it provides greater recentring.

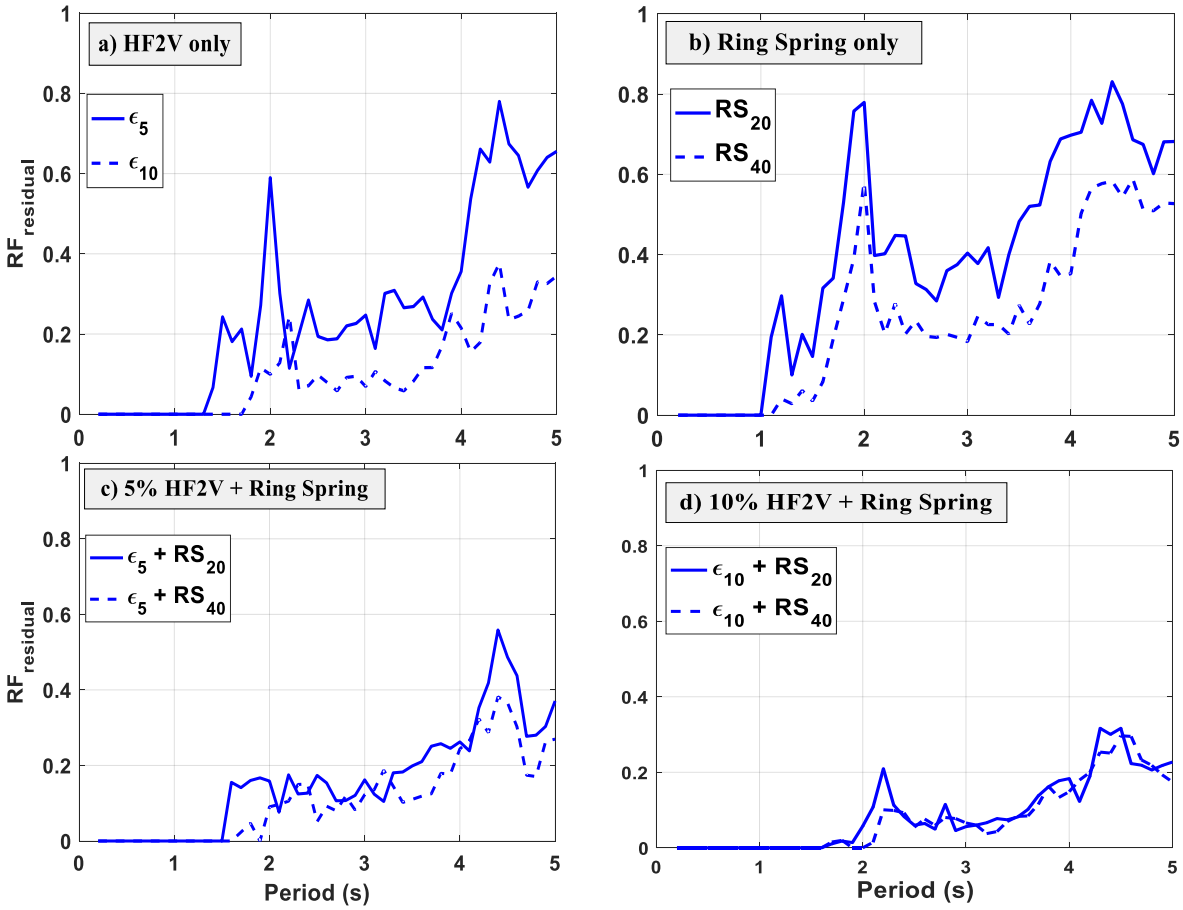


*Figure 28: Residual displacement RF results for: a) HFV2 only; b) Ring Spring only; c) 5% HF2V with both ring springs; and d) 10% HF2V with both ring springs*

## Base Shear Results

Base shear RFs are shown in Fig. 29 where a reduction in base shear is observed for structures with periods less than approximately *1 sec*. However, for longer period structures, significantly increased base shear is observed, as a consequence of the resistive and restoring forces imposed by the supplemental components. Such an increase suggests that the forces added to reduce displacements outweigh the reduced structural forces due to those displacement reductions. Comparing the response spectra with and without HF2V shows that the base shear is largely dominated by the contribution of the HF2V devices due to their dominant contribution to displacement reductions in Figure 27. In addition, the added base shear in the case of the structure with ring spring only, is largely independent of its natural period.

To determine the contribution of individual components to the maximum base shear, percentage share of each component (nonlinear structural restoring force [$F_S$], HF2V force [$F_{HF2V}$], and ring spring force [$F_{RS}$]) to the overall base shear is shown in Fig. 30. The plots are generated similar to the way response spectra were created and shown in previous figures i.e. the contribution of each component at the instance of maximum base shear during a particular ground motion input is recorded. Then the data obtained from all 20 earthquakes are then plotted using geometric mean values.

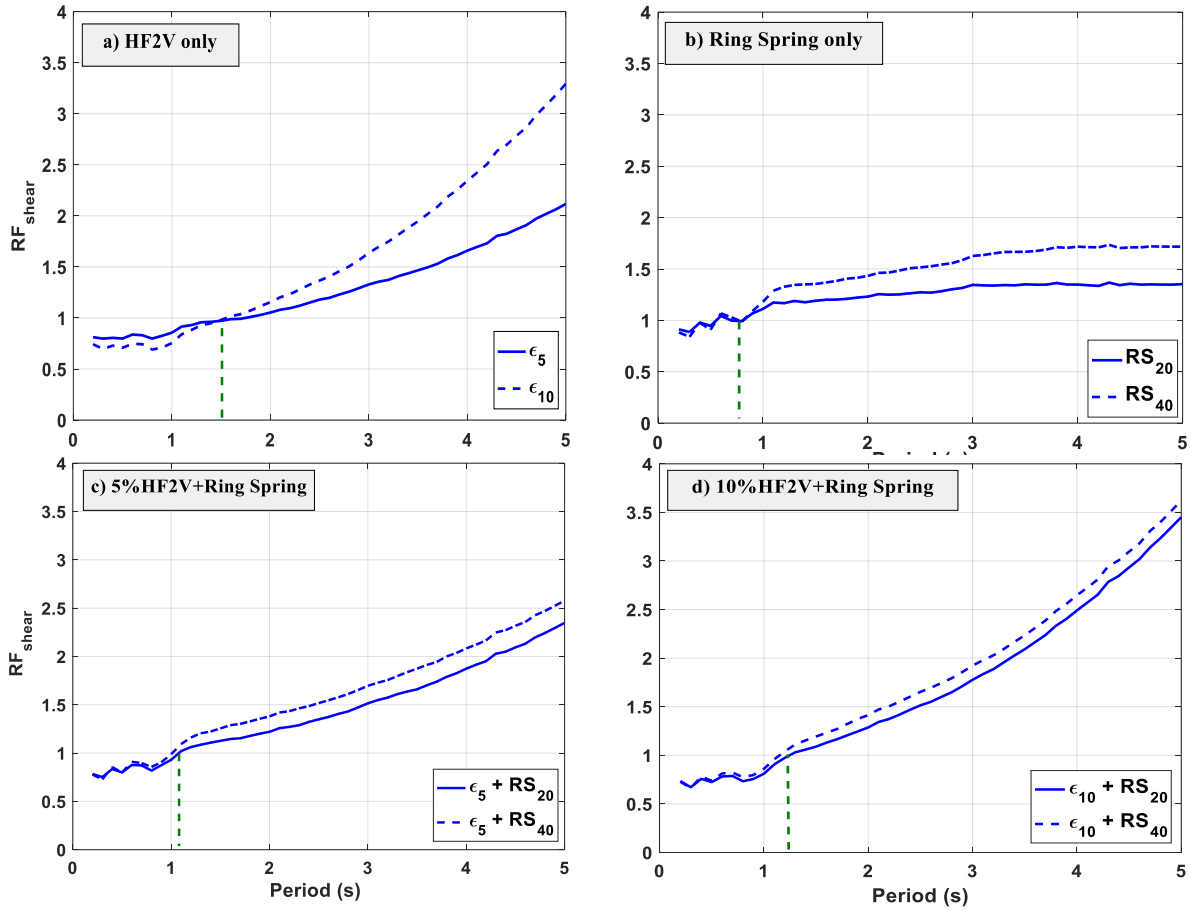


*Figure 29: Base shear RF results for: a) HFV2 only; b) Ring Spring only; c) 5% HF2V with both ring springs; and d) 10% HF2V with both ring springs. Green vertical dashed lines show the period for $RF_{shear}=1$*

A period-dependent increasing trend is witnessed for the HF2V force which is mainly associated with its velocity-dependent behaviour (Figs. 30(a) and 30(c)-(d)). The relative contribution of structural restoring force decreases as the period of the structure gets longer since the structural stiffness of the system decreases with an increase in natural period. Moreover, the base shear contribution of the ring spring in the hybrid device shows relatively low sensitivity to the natural period of the structure with ~15% for $RS_{20}$ and ~20% for $RS_{40}$.

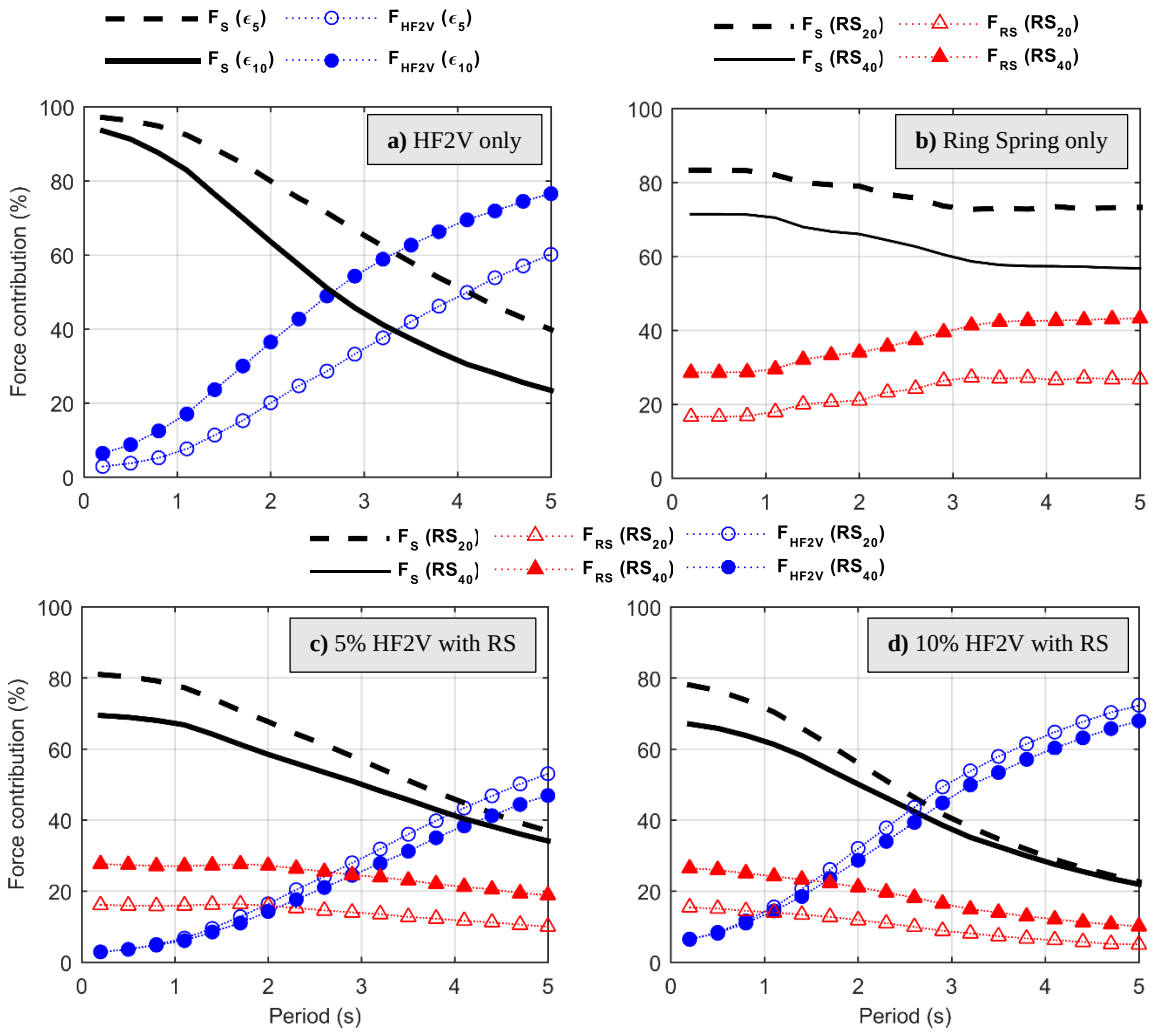


*Figure 30: Base shear components: a) HFV2 only; b) Ring Spring only; c) 5% HF2V with both ring springs; and d) 10% HF2V with both ring springs*

# Discussion

Displacement response reductions are mainly dominated by the effect of HF2V device indicating that using larger device ($\varepsilon_{10}$) without ring spring is favourable based on displacement alone. However, with regards to residual displacement, both components show a robust performance. Results suggest that an excellent reduction in residual displacement is achieved by using a hybrid device reducing the need for any post-earthquake remediation on a structure using these devices.

However, reductions come at a cost. Base shear response is dominated by the contribution of HF2V force and ring springs impose the smaller forces to the structure. Considering base shear alone, the smaller ring spring only ($RS_{20}$) is the best option to add to the structure. Considering all three response parameters evaluated, using a hybrid device that consists of 5% HF2V device ($\varepsilon_5$) and 40% ring spring ($RS_{40}$) seems to generate a more optimal response spectra for performance versus increased base shear. The overall results allow any series of choices to be assessed parametrically as the stiffness ratios and $\varepsilon$ values span a reasonably achievable range for these devices (Rodgers *et al.*, 2007; Rodgers *et al.*, 2008; Khoo *et al.*, 2013; Bishay-Girges and Carr, 2014).

The SDOF design spectrum analysis is limited by the number of degrees of freedom. However, the analysis approach using RFs is entirely generalizable. For multi-degree-of-freedom (MDOF) systems representing multi-storey structures the reduction factors would be calculated in a similar fashion but there would be more of them depending on the number of storeys. For displacement at every storey of an 8-storey frame, there would be 8 RFs. However, if the structure was first mode dominant in response, as is typical, then the top storey deflection and single RF, similar to this analysis would suffice. In this case, any complex MDOF case is often quite specific to a single structure, where the approach here is generalizable to initial design of many possible structures. The analysis of how these devices influence the response of larger MDOF structures in the presence of higher mode effects is an important aspect of future work.

Experimental verification is critical. However, this paper first establishes the potential for these hybrid devices before engaging in an extensive experimental test series. Because they are hybrid devices, experimental outcomes for a given device is the combination of the force capacities of both devices as a function of the input displacement and velocity. Thus, while a hybrid device has not been experimentally validated, there is extensive device level and in-situ validation of HF2V devices (Rodgers *et al.*, 2008) and of ring springs (Khoo *et al.*, 2012; Khoo *et al.*, 2013). These outcomes show that the devices behave according to the models used in this paper in Eqs. (10)-(17) for modelling them. Thus, while the paper does not include experimental validation of a hybrid device, there is confidence that upcoming validation experiments, which were outside the length and scope of this article, will behave similarly.

# Conclusions

Comprehensive simulation of the structural response of a nonlinear hysteretic structure across a range of earthquakes has shown that significant reductions in peak displacement response can be achieved using realistic configurations of hybrid damping devices. Based on the investigations described, the following conclusions can be drawn:

- Both the HF2V device and ring spring can modify the response metrics of the nonlinear system in terms of peak and residual displacements as a result of their damping capacity.
- Peak displacement reduction factors are mainly controlled by the impact of HF2V devices particularly for larger periods.
- Separately, either HF2V devices or ring springs reduce the residual displacements. However, combining them in a hybrid device results in even greater reductions of residual displacements giving the structure high self-centring ability.
- Using supplemental damping devices can result in reduced base shear force only for low period structures. For higher periods, noticeably magnified base shear forces are witnessed in the structure.
- The increase in base shear is dominated by the contribution of HF2V component. Thus, from the base shear point of view, smaller HF2V is preferred for a hybrid device.
- Using ring spring only results in considerably lower residual displacements, with minimal increase in base shear. Thus, from a residual displacement viewpoint, using ring spring only is preferred over a hybrid device.

# References


Bacht, T., Chase, J.G., MacRae, G., Rodgers, G.W., Rabczuk, T., Dhakal, R.P. and Desombre, J. (2011), "HF2V dissipator effects on the performance of a 3 storey moment frame", *Journal of Constructional Steel Research*. **67**(12), 1843-1849.

Bazzurro, P., Cornell, C., Menun, C. and Motahari, M. (2004). "Guidelines for seismic assessment of damaged buildings", *Proceedings of the 13th World Conference on Earthquake Engineering, Vancouver, Canada*.

Bhunia, D., Prakash, V. and Pandey, A.D. (2012), "A study on the behaviour of coupled shear walls", *Structural Engineering and Mechanics*. **42**(5), 645-675.

Bishay-Girges, N.W. and Carr, A.J. (2014), "Ring spring dampers: Passive control system for seismic protection of structures", *Bulletin of the New Zealand Society for Earthquake Engineering*. **47**(3).

Chang, S.E. (2010), "Urban disaster recovery: a measurement framework and its application to the 1995 Kobe earthquake", *Disasters*. **34**(2), 303-327.

Chiou, D.J., Hsu, W.K., Chen, C.W., Hsieh, C.M., Tang, J.P. and Chiang, W.L. (2011), "Applications of Hilbert-Huang transform to structural damage detection", *Structural Engineering and Mechanics*. **39**(1), 1-20.

Chopra, A.K. and Goel, R.K. (2001), "Direct Displacement-Based Design: Use of Inelastic vs. Elastic Design Spectra", *Earthquake Spectra*. **17**(1), 47-64.

Cousins, W. and Porritt, T. (1993), "Improvements to lead-extrusion damper technology", *Bulletin of the New Zealand National Society for Earthquake Engineering*. **26**(3), 342-348.

Cousins, W., Robinson, W. and McVerry, G. (1991). "Recent developments in devices for seismic isolation", *Proc. Pacific Conference on Earthquake Engineering*.

Elnashai, A.S., Borzi, B. and Vlachos, S. (2004), "Deformation-based vulnerability functions for RC bridges", *Structural Engineering and Mechanics*. **17**(2), 215-244.

Erasmus, L. (1988), "Ring springs on holding-down bolts for seismic energy dissipation", *Transactions of the Institution of Professional Engineers New Zealand: Civil Engineering Section*. **15**(2), 41-47.

Ewing, C.M., Guillin, C., Dhakal, R.P. and Chase, J.G. (2009), "Spectral analysis of semi-actively controlled structures subjected to blast loading", *Structural Engineering and Mechanics*. **33**(1), 79-93.

Filiatrault, A., Tremblay, R. and Kar, R. (2000), "Performance evaluation of friction spring seismic damper", *Journal of Structural Engineering*. **126**(4), 491-499.

Gledhill, S., Sidwell, G. and Bell, D. (2008). "The damage avoidance design of tall steel frame buildings—Fairlie terrace student accommodation project, Victoria University of Wellington", *New Zealand Society of Earthquake Engineering Annual Conference*.

Hamid, N.H. and Mander, J. (2014), "Damage avoidance design for buildings", *KSCE Journal of Civil Engineering*. **18**(2), 541-548.

Hill, K.E. (1995), *The Utility of Ring Springs in Seismic Isolation Systems: A Thesis Submitted for the Degree of Doctor of Philosophy* University of Canterbury, New Zealand.

Kaiser, A., Holden, C., Beavan, J., Beetham, D., Benites, R., Celentano, A., Collett, D., Cousins, J., Cubrinovski, M. and Dellow, G. (2012), "The Mw 6.2 Christchurch earthquake of February 2011: preliminary report", *New Zealand journal of geology and geophysics*. **55**(1), 67-90.

Kar, R., Rainer, J. and Lefrançois, A. (1996), "Dynamic properties of a circuit breaker with friction-based seismic dampers", *Earthquake spectra*. **12**(2), 297-314.

Khoo, H.-H., Clifton, C., Butterworth, J. and MacRae, G. (2013), "Experimental Study of Full-Scale Self-Centering Sliding Hinge Joint Connections with Friction Ring Springs", *Journal of Earthquake Engineering*. **17**(7), 972-997.

Khoo, H.-H., Clifton, C., Butterworth, J., MacRae, G., Gledhill, S. and Sidwell, G. (2012), "Development of the self-centering Sliding Hinge Joint with friction ring springs", *Journal of Constructional Steel Research*. **78** 201-211.

Khoo, H., Clifton, G., Butterworth, J. and MacRae, G. (2012). "Experimental studies of the self-centering Sliding Hinge Joint", *NZSEE Conference, Christchurch, New Zealand*.

Kordani, R., Rodgers, G. and Chase, J. (2015). "Response analysis of hybrid damping device with self-centring", *New Zealand Society of Earthquake Engineering Conference*.

Luco, N., Bazzurro, P. and Cornell, C.A. (2004). "Dynamic versus static computation of the residual capacity of a mainshock-damaged building to withstand an aftershock", *Proceedings of the 13th world conference on earthquake engineering*.

Mander, J.B. and Cheng, C.-T. (1997), *Seismic resistance of bridge piers based on damage avoidance design*, U.S. National Center for Earthquake Engineering Research (NCEER)

Maniyar, M.M., Khare, R.K. and Dhakal, R.P. (2009), "Probabilistic seismic performance evaluation of non-seismic RC frame buildings", *Structural Engineering and Mechanics*. **33**(6), 725-745.

Menegotto, M. and Pinto, P. (1973), *Method of Analysis for Cyclically Loaded R. C. Plane Frames Including Changes in Geometry and Non-Elastic Behavior of Elements under Combined Normal Force and Bending*,

Polese, M., Di Ludovico, M., Prota, A. and Manfredi, G. (2013), "Damage-dependent vulnerability curves for existing buildings", *Earthquake Engineering & Structural Dynamics*. **42**(6), 853-870.

Rodgers, G., Denmead, C., Leach, N., Chase, J. and Mander, J. (2006), "Spectral evaluation of high force-volume lead dampers for structural response reduction".

Rodgers, G.W., Chase, J.G., Mander, J., Dhakal, R.P. and Solberg, K.M. (2007). "DAD Post-Tensioned Concrete Connections with Lead Dampers: Analytical Models and Experimental Validation", *8th Pacific Conference on Earthquake Engineering*.

Rodgers, G.W., Chase, J.G., Mander, J.B., Leach, N.C. and Denmead, C.S. (2007), "Experimental development, tradeoff analysis and design implementation of high force-to-volume damping technology", *Bulletin of the New Zealand Society for Earthquake Engineering*. **40**(2), 35-48.

Rodgers, G.W., Mander, J.B. and Chase, J.G. (2011), "Semi-explicit rate-dependent modeling of damage-avoidance steel connections using HF2V damping devices", *Earthquake Engineering & Structural Dynamics*. **40**(9), 977-992.

Rodgers, G.W., Mander, J.B., Chase, J.G., Dhakal, R.P., Leach, N.C. and Denmead, C.S. (2008), "Spectral analysis and design approach for high force-to-volume extrusion damper-based structural energy dissipation", *Earthquake Engineering & Structural Dynamics*. **37**(2), 207-223.

Rodgers, G.W., Solberg, K.M., Chase, J.G., Mander, J.B., Bradley, B.A., Dhakal, R.P. and Li, L. (2008), "Performance of a damage-protected beam-column subassembly utilizing external HF2V energy dissipation devices", *Earthquake Engineering & Structural Dynamics*. **37**(13), 1549-1564.

Rodgers, G.W., Solberg, K.M., Mander, J.B., Chase, J.G., Bradley, B.A. and Dhakal, R.P. (2012), "High-force-to-volume seismic dissipators embedded in a jointed precast concrete frame", *J. Struct. Eng.*, **138**(3), 375-386.

Ruiz-García, J. and Aguilar, J.D. (2015), "Aftershock seismic assessment taking into account postmainshock residual drifts", *Earthquake Engineering & Structural Dynamics*. **44**(9), 1391-1407.

Salari, N. and Asgarian, B. (2015), "Seismic response of steel braced frames equipped with shape memory alloy-based hybrid devices", *Structural Engineering and Mechanics*. **53**(5), 1031-1049.

Somerville, P.G. and Venture, S.J. (1997), *Development of ground motion time histories for phase 2 of the FEMA/SAC steel project*, SAC Joint Venture

Subramanian, K. and Velayutham, M. (2014), "Seismic performance of lateral load resisting systems", *Structural Engineering and Mechanics*. **51**(3), 487-502.

Yang, M., Xu, Z. and Zhang, X. (2015), "Experimental study on lead extrusion damper and its earthquake mitigation effects for large-span reticulated shell", *Steel Compos. Struct.*, **18**(2), 481-496.

Yon, B., Sayın, E. and Koksal, T.S. (2013), "Seismic response of buildings during the May 19, 2011 Simav, Turkey earthquake", *Earthquakes and Structures*. **5**(3), 343-357.

# Shake Table Tests of Damping Devices

## Executive Summary

In the previous sections, component tests of the damping devices have been undertaken and structural-level modelling has been completed to determine the likely response of a structure fitted with this type of supplemental damping system. Finally, to combine these aspects, the devices developed were included in a 14-tonne two-storey, low-damage steel frame structure that underwent testing on the University of Auckland shake table test facility. This important final step in the research combines the key theme of the previous two sections, to determine if the predicted response behaviour at the structural-level matches the predictions made from the computational study.

This section outlines the experimental validations of a passive Direction and Displacement Dependent (D3) viscous damping device. The passive D3 viscous device produces viscous damping in any individual or multiple quadrants of the force-displacement response. The results provide the design approach, device characterization and validation for this novel device design. The effectiveness of both a 2-4 configuration of a D3 viscous damping device, (providing damping in only quadrants 2 and 4 of the force-displacement response plot), and a 1-3 configuration of D3 viscous damper devices are compared with the performance of a typical viscous damper. An experimental study of a 1/2 scale two storey steel frame building with passive 2-4 configuration of D3 dampers is subjected to shake table testing and the seismic performance of the supplemental damping system is assessed. The overall results show that the 2-4 D3 viscous damper can simultaneously reduce displacement response base shear force and acceleration and is therefore a robust means to mitigate the risk of damage to the structure, foundation and contents for either new designs or retrofit.

## Introduction

Fluid viscous damping is a way of adding energy dissipation to the lateral motion of a structural system without involving major building modifications. However, the addition of the dampers into the building frame can lead to an increase in the maximum base shear and column axial forces, which, in practice, may require strengthening of columns and the foundations. Hence, any device that can robustly dissipate energy without increasing column and base shear demands would offer potential advantages.

A nonlinear structure during sinusoidal loading with a standard viscous device has hysteresis loop definitions like those schematically shown in a Fig. 31a, where the elliptic force-deflection response due to the viscous damper is added to the nonlinear force deflection response. A standard viscous damper provides a robust, well-understood method to dissipate significant energy. However, the resulting base-shear force can be increased for structures with this type of response behaviour, as shown in the schematic.

To address this problem, Hazaveh et al [5,10] introduced the Direction Dependent Dissipation (D3) device and examine two types of D3 viscous device, a 1-3 and 2-4, to sculpt hysteretic behavior. The 2-4 configuration of the D3 device can reduce the base-shear demand by providing damping forces only in the second and forth quadrants of the force deformation plot, resisting motion only toward a zero-displacement configuration (Fig. 31c). Therefore, the 2-4 D3 device appeared to be an appealing solution for reducing seismic response in displacement (structural demand) and base shear (foundation demand).

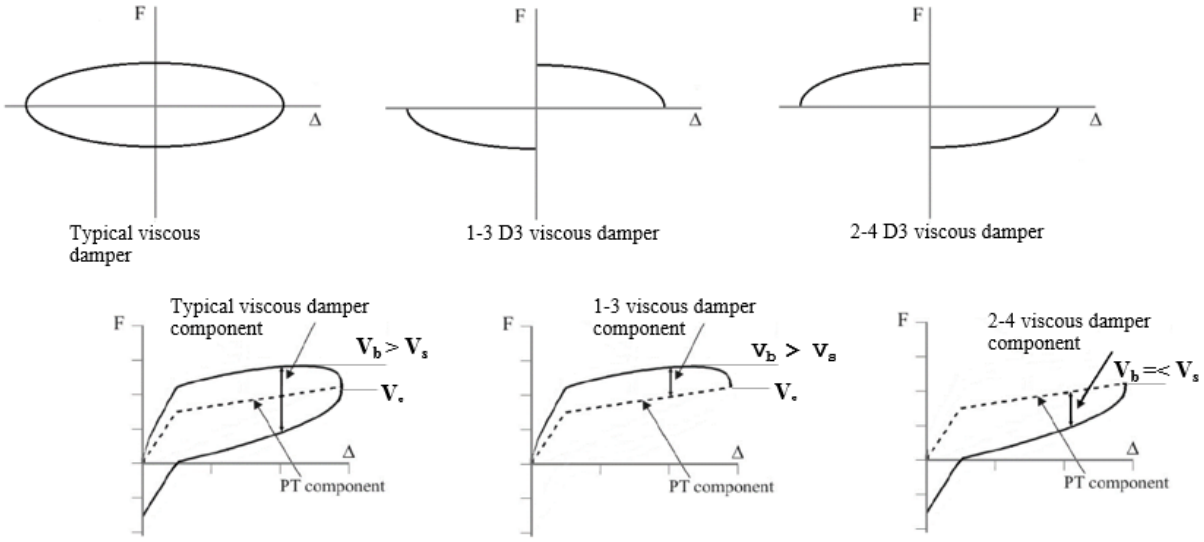


*Figure 31: Schematic hysteresis for a typical, 1-3, and 2-4 viscous damper device, $V_b$ = total base shear, $V_S$ = base shear for undamped structure. $V_b > V_S$ indicates an increase due to the additional damping.*

In this study, the new passive D3 viscous device can provide viscous damping in any individual or multiple quadrants of the force-displacement response is introduced. The effectiveness of a 2-4 configuration of a D3 viscous damping device is compared numerically with the performance of a typical viscous damper and a 1-3 D3 viscous damper devices. Then, experimental validation of a prototype device is undertaken using an MTS810 hydraulic test machine. The results provide the design approach, device characterization and validation for this novel device design. Finally, an experimental study of a 1/2 scale two storey steel frame building with passive 2-4 configuration of D3 dampers is subjected to shake table testing and the seismic performance of the supplemental damping system is assessed.

The overall results show that the 2-4 D3 viscous damper can simultaneously reduce displacement response base shear force and acceleration and is therefore a robust means to mitigate the risk of damage to the structure, foundation and contents for either new designs or retrofit.

# Numerical Study

This study investigates the relative effectiveness of a traditional viscous damper, and the 1-3 and 2-4 D3 viscous dampers on the seismic response of self-centering SDOF structural systems with periods T=0.1- 4.5 sec. The self-centering rocking behaviour is modelled numerically with an idealized bi-linear elastic spring [11]. The analysis of each test structure utilizes all 60 earthquakes from the 3 earthquake suites of the SAC project [12]. Each suite is comprised of 10 different time histories with two orthogonal directions for each history. The 3 suites contain ground motions having probabilities of exceedance of 50%, 10% and 2% in 50 years in the Los Angeles region, denoted the low, medium and high suites, respectively.

Figure 32 shows the median structural displacement ($RF_{Sd}$) and base shear ($RF_{vb}$) reduction factors versus period for the self-centering SDOF structures (T=0.1- 4.5 sec). As expected, the typical viscous damper (1-4 device) offers the greatest displacement reduction as it has the biggest area enclosed within the device hysteretic loop in Figure 32, but increases the overall base shear by the largest amount for almost all periods, in recompense. For example, for a period of 3.0 sec, $RF_{vb} \approx 3.0$ for the typical viscous device, indicating total base shear with the viscous damper is three times that of the uncontrolled (no device) case. Similarly, the 1-3 device has $RF_{Sd} < 1.0$ and $RF_{vb} > 1.0$ for most periods. However, the 1-3 viscous device reduces displacement less than the 1-4 typical viscous damper, as the area enclosed with the device hysteretic loop is approximately half the size, as shown in Figure 31.

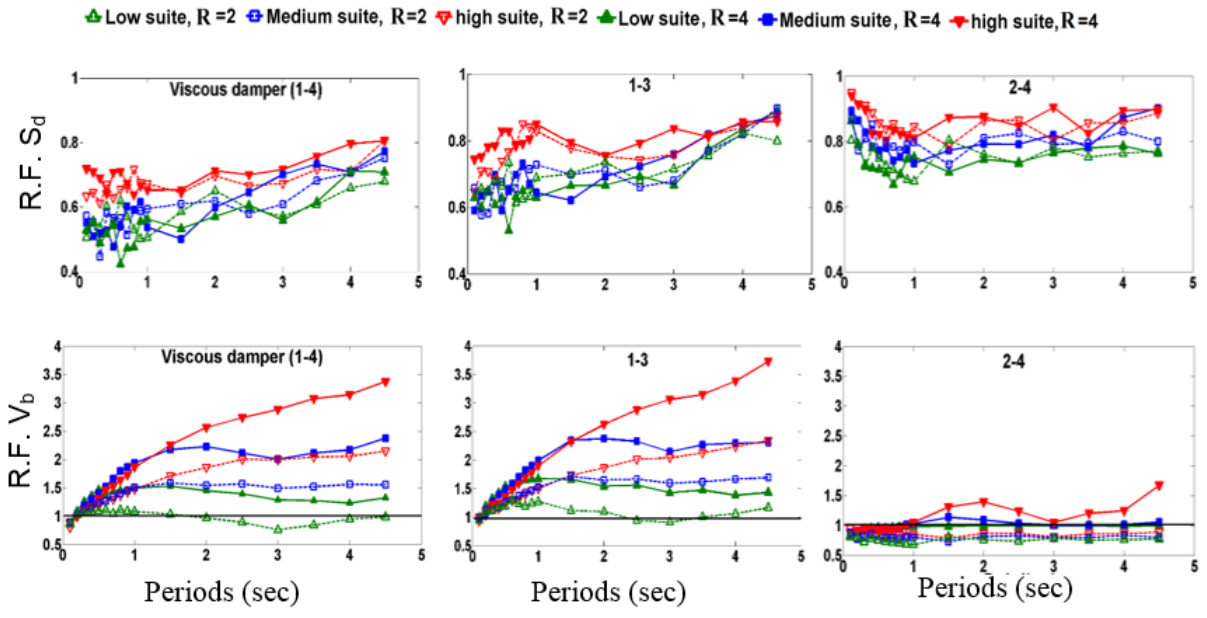


*Figure 32: The median damping reduction factor of structural displacement, total base shear and acceleration of structures with periods 0.1sec to 4.5 sec and ductility (R) of 2.0 and 4.0 with three type viscous devices, with values of 5% additional damping under low, medium and high suite ground motion.*

In contrast, the 2-4 viscous device has $RF_{Sd}$ <1.0 and $RF_{vb}$ <1.0 in almost all cases. Overall, the 2-4 viscous device provides $RF_{sd}$ and $RF_{vb}$ ≤ 1.0 at levels that are relatively constant across periods. The 2-4 viscous damper approach thus offers the minimum variability in median level risk and thus the greatest robustness across structural periods, to a level not available from the other two devices considered. More specifically, the 2-4 viscous damper offers minimal risk of increased foundation demand along with reduced displacement demands.

# Experimental Component Testing

Experimental validation of a 2-4 Displacement Direction Dependent (D3) dissipation device that provides viscous damping in two quadrants is undertaken using an MTS810 hydraulic test machine. Sinusoidal displacement inputs provide a range of velocity inputs and device forces used to characterize the damping behaviour of the prototype and illustrate the ability to provide controllable viscous damping in any single or multiple quadrant(s) of the force-displacement response.

The damping device was modified in two steps, by first modifying the piston then by modifying the cylinder to have a passive single quadrant viscous damper. The prototype piston was constructed with 2 sets of independent orifices. These orifices can be individually blocked to experimentally test different configurations and damping levels. To provide one way flow and thus direction dependent damping, a flat ring plate was added to the piston design to cover the one set orifices when the piston is moving toward the side with the ring, as shown in Figure 33.

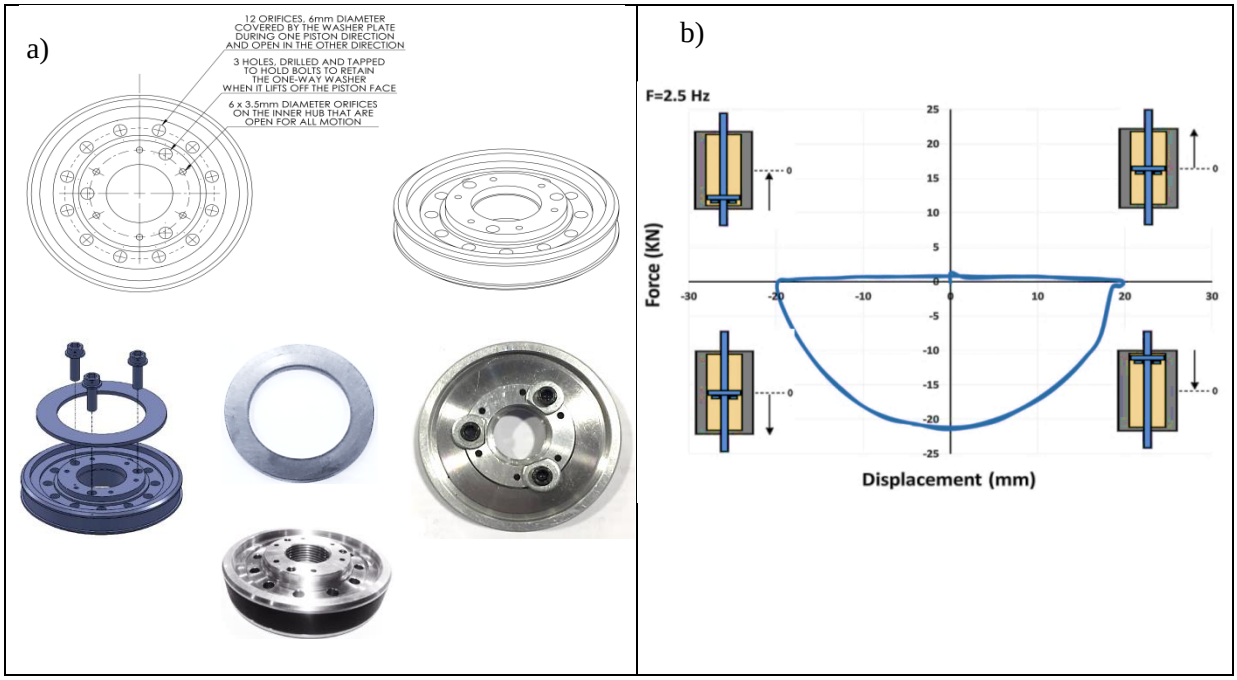


*Figure 33: a) Scheme and photo of the modified piston, (b) Force-displacement of the device showing half the hysteresis loop (2-3 quadrants only) of a viscous damper when 6 orifices are open under sinusoidal loading with frequency 2.5 Hz and amplitude 20 mm.*

The next step is a device with damping in only one quadrant of the force-displacement plot. To achieve a single quadrant hysteresis loop, requires displacement or location dependent damping so that damping is only produced in one half of the device cylinder. To achieve this goal, the internal cylinder diameter is increased over half of the device, to enable the fluid to flow through an annular gap around the piston circumference in this half of the cylinder, negating any damping when moving in either direction. Therefore, when the piston is located in the area that has larger cylinder bare diameter the device produces only minimal damping forces. The design illustration is shown in Figure 34.

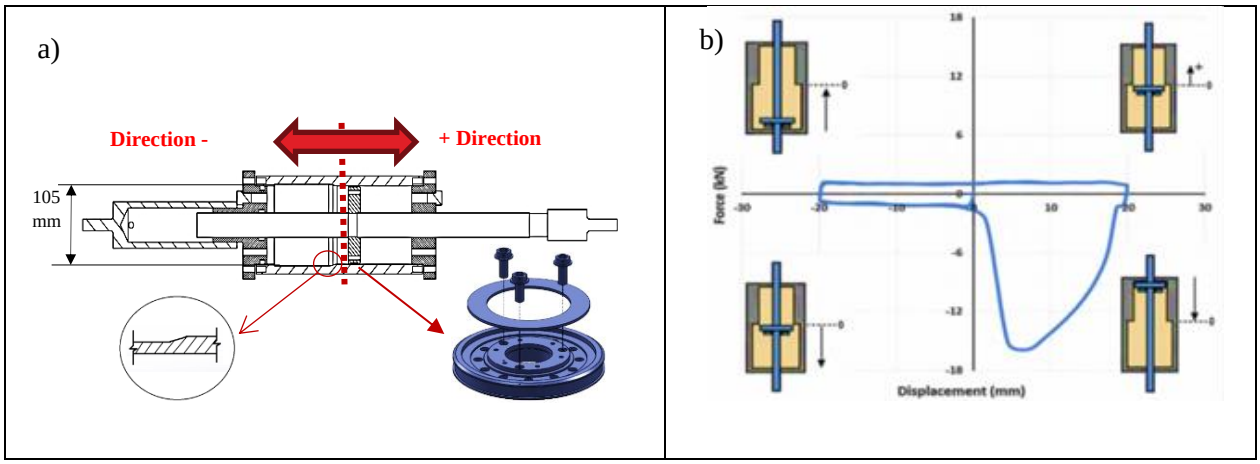


*Figure 34: a) Scheme of the modified cylinder. b) Step-by-step representation of position of the modified piston in the modified cylinder under a sinusoidal loading.*

To obtain 1-3 or 2-4 behaviour in an entirely passive, not semi-active, manner is thus just a matter of either: a) combining multiple single-quadrant devices in series configuration with shared shaft or in a parallel configuration with a shared connection, or b) creating a combined device design with two pistons and a shared shaft in a single cylinder with 2 stepped portions of the cylinder bore. Hence, there is no specific limitation to the type of damping hysteresis loop that might be obtained in terms of which quadrants or parts of quadrants experience viscous damping and which do not. Figure 35 shows the 2-4 D3 viscous device design illustration.

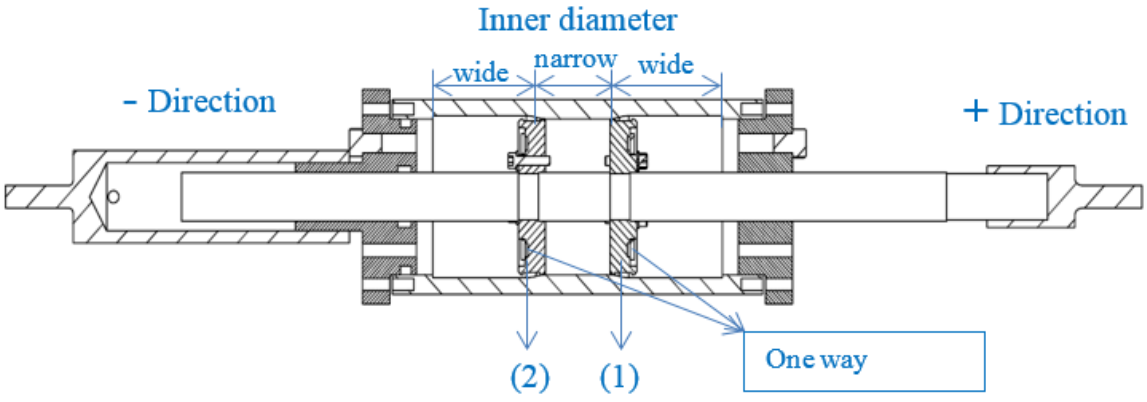


*Figure 35: 2-4 configuration of D3 viscous device prototype*

Figure 36 shows the resulting experimental force-displacement under sinusoidal loading with input amplitude 35 mm and a range of input frequencies. It is clear a 2-4 device behaviour is obtained. Experimental validation of a proof of concept device validates the direction dependent and displacement dependent damping has been obtained, and confirms the capability of providing this viscous damping entirely passively in relatively low device cost design.

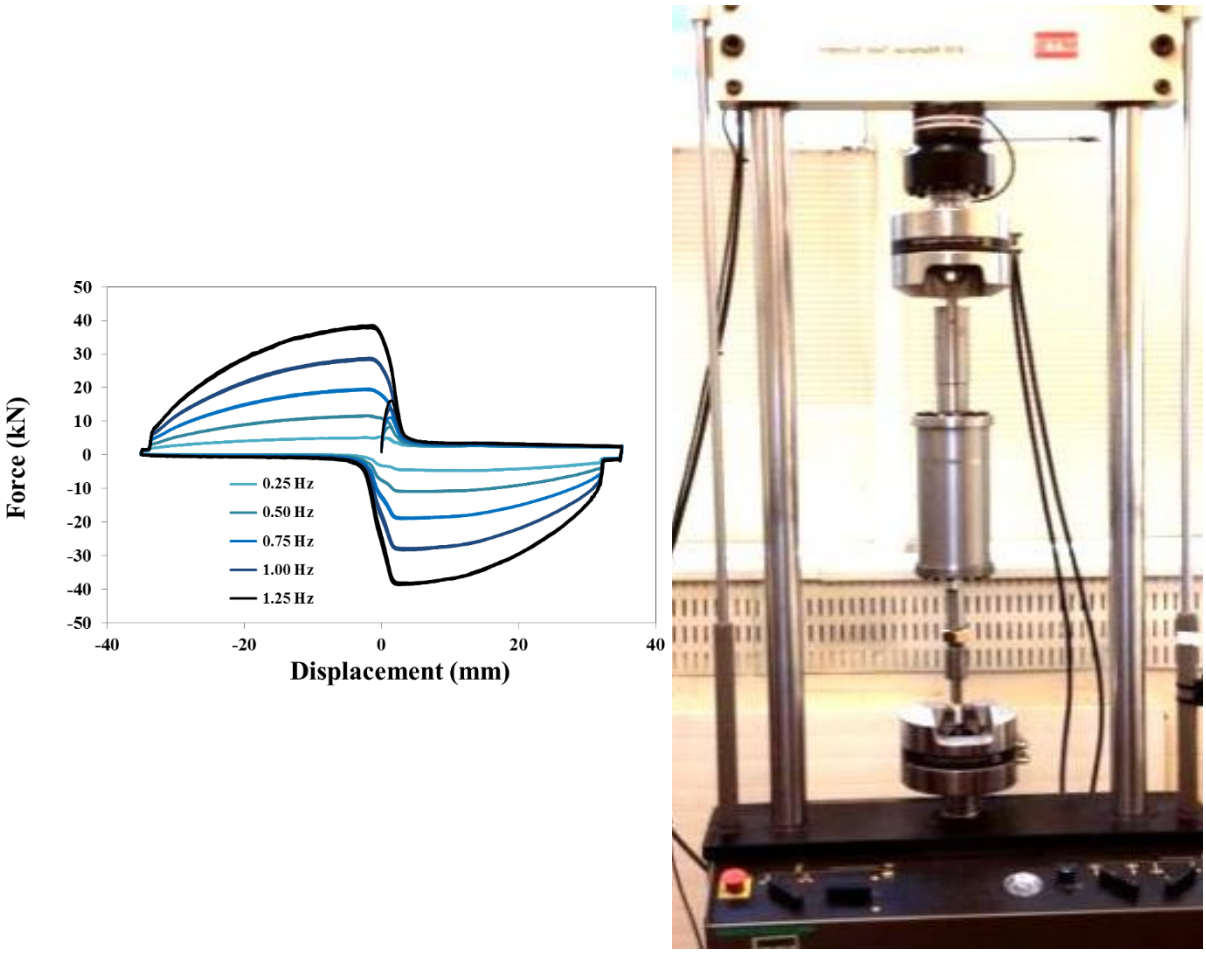


*Figure 36: Force-displacement of the 2-4 D3 device with 3 orifices open when providing damping force under sinusoidal input loading with different frequencies and an input amplitude 35 mm. The experimental test setup in the MTS-810 machine.*

# Shake Table Testing

The numerical structural model and the experimental component testing were then experimentally validated in combination via the seismic performance of a 1/2 scale, two storey steel frame building with passive 2-4 D3 dampers subjected to uni-directional shake table testing. The test specimen is composed of two steel frames with Asymmetric Friction Connections (AFC) [13-16] in the column base and beam-to-column joints, as shown in Figure 37. In the transverse direction, the two frames are joined by short transverse beams. The length of the beams, columns and the amount of the mass at each floor are provided in Table 9.

*Table 9: Properties of the two-storey test buildings*

| Items | Properties |
|---|---|
| Inter-storey height [m] | 1.6 |
| Bay length [m] | 3.2 |
| Building width [m] | 2 |
| Mass per floor [ton] | 6.5 |
| Column Section | 100 UC 14.8 |
| Beam Section | 100 UC 14.8 |

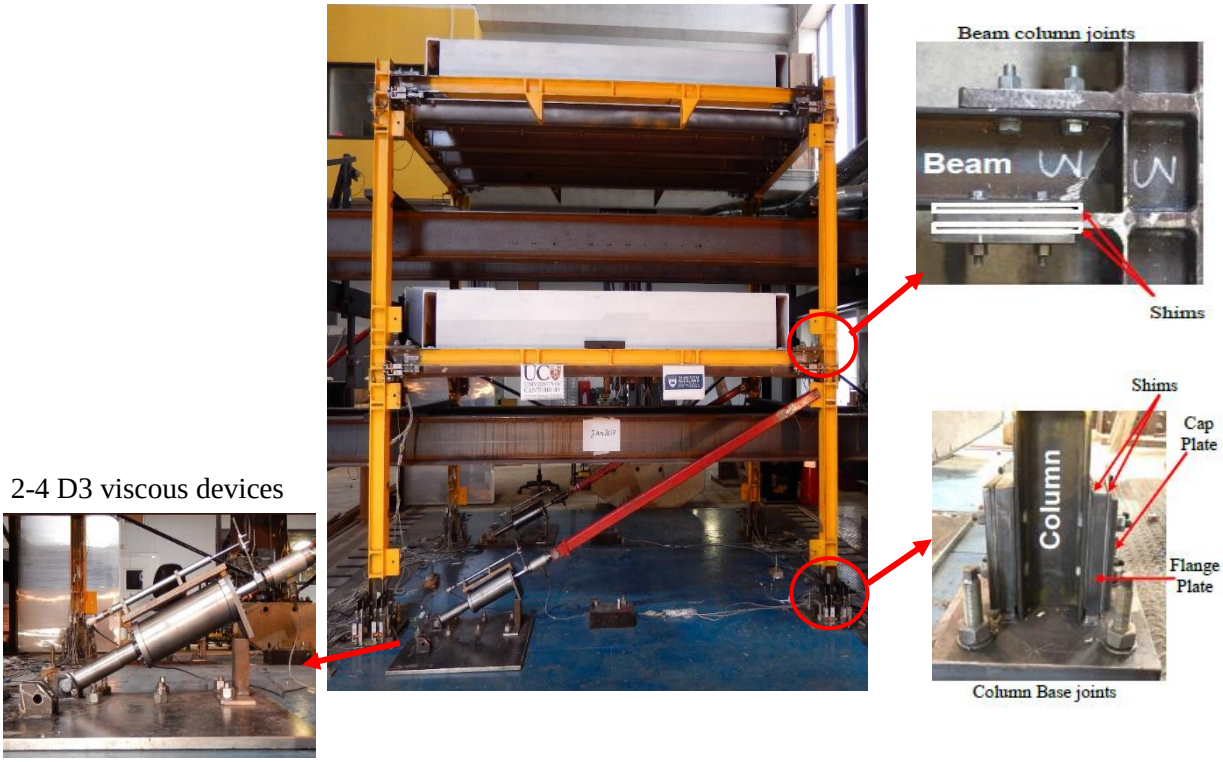


*Figure 37: Test building constructed frame. Two steel frames with asymmetric friction connections (AFC) in the column base and beam-to-column joints. Constructed test building frame was applied with two 2-4 D3 viscous damper prototypes.*

Figure 38a shows the maximum displacement of the structure without any dissipation devices is approximately 98 mm for the Kobe earthquake input. The resulting maximum drift at the roof level is about 3.04%, which is larger than the desired value of 2.5%. To improve the structural performance and reduce the maximum drift, the 2-4 configuration of D3 viscous damper was used as shown Figure 37.

After applying two 2-4 D3 viscous dampers, the drift is reduced approximately 40% to 1.83%. Using the 2-4 viscous damper decreased the structural drift, while decreasing the total base shear and acceleration, as seen in Fig. 35b-c. In particular, Figure 38b shows the hysteresis loop of the structure before and after using the 2-4 viscous damper. The hysteresis loop of the 2-4 D3 viscous damper is shown in Figure 38d. These results show that applying damping in only quadrants 2 and 4 not only reduces the displacements of the structure, but, as expected and desired, it also reduces the base shear. The accelerations (Figure 38c) are also reduced. Hence, there is no additional foundation demand, structural displacement demand or damage to contents, as seen in the accelerations, to improve the structural performance with these devices.

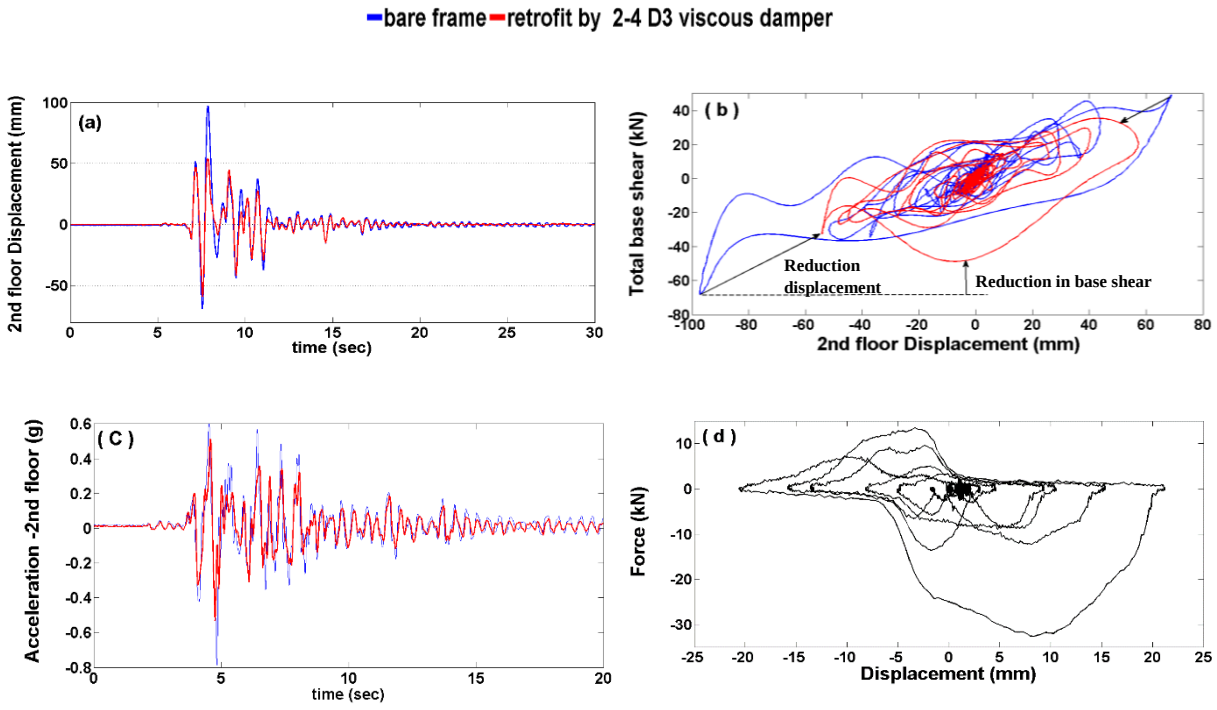


*Figure 38: Structural response under Kobe earthquake before and after using the 2-4 D3 viscous damper, (a) Displacement of second floor (b) hysteresis loop of the structure, (c) acceleration of second floor (d) force-displacement of the 2-4 D3 viscous damper.*

# Conclusions

This section presents computational and experimental studies on improving seismic structural performance using novel Displacement and Direction Dependent (D3) viscous devices. These proposed devices offer the adaptability of semi-active devices in an entirely passive device design, and thus include the high reliability and low complexity of passive devices. The effectiveness of a 2-4 configuration of a D3 viscous damping device is compared with the performance of a typical viscous damper. Given the potential and link to standard design procedures, the D3 device design concept is presented and experimental tests undertaken on a prototype device. Finally, experimental validation using the proposed device is undertaken by shake table tests of a half scale two storey steel structure. The results show that using the 2-4 D3 viscous damper could reduce the displacement and inter-storey drift to reach the desired design value without increasing base shear and floor accelerations. Therefore, there is no additional foundation demand and there is a potential reduction in content damage. The overall results show that simultaneous reductions in displacement, base-shear and displacement demand for nonlinear structural deformation is available with the 2–4 D3 viscous fluid damper.

# References


1. A. Filiatrault, R. Tremblay, A. Wanitkorkul, Performance evaluation of passive damping systems for the seismic retrofit of steel moment-resisting frames subjected to near-field ground motions. Earthquake Spectra 2001; 17(3): 427-456.
2. P. Uriz, A.Whittaker, Retrofit of pre-Northridge steel moment-resisting frames using fluid viscous dampers. The Structural Design of Tall and Special Buildings. 2001; 10(5): 371-390.
3. H. K. Miyamoto, J. Singh, Performance of structures with passive energy dissipators. Earthquake spectra. 2002; 18(1): 105-119.
4. M. Martinez-Rodrigo, M. Romero, An optimum retrofit strategy for moment resisting frames with nonlinear viscous dampers for seismic applications. Engineering Structures. 2003; 25(7): 913-925.
5. N.K. Hazaveh, S. Pampanin, G. Rodgers, J. Chase, Novel Semi-active Viscous Damping Device for Reshaping Structural Response. Conference: 6WCSCM (Sixth World Conference of the International Association for Structural Control and Monitoring), 2014; Spain.
6. N.K. Hazaveh, J.G. Chase, G.W. Rodgers, S. Pampanin, Control of Structural Response with a New Semi-Active Viscous Damping Device. 8th International Conference on Behavior of Steel Structures in Seismic Areas, 2015; China.
7. N.K. Hazaveh, S. Pampanin, G.W. Rodgers, J.G. Chase, Design and experimental test of a Direction Dependent Dissipation (D3) device with off-diagonal (2-4) damping behaviour. NZSEE, 2016; Christchutch, New Zealand.
8. N.K. Hazaveh, G.W. Rodgers, J.G. Chase, S. Pampanin, Reshaping Structural Hysteresis Response with Semi-active Viscous Damping. Bulletin of Earthquake Engineering, 2016; in press.

9. N.K. Hazaveh, G.W. Rodgers, S. Pampanin, J.G. Chase, Damping reduction factors and code-based design equation for structures using semi-active viscous dampers. Earthquake Engineering & Structural Dynamics, (2016) 45(15): 2533-2550.

10. N.K. Hazaveh, G.W. Rodgers, J.G. Chase, S. Pampanin, Experimental Test and Validation of a Direction and Displacement Dependent (D3) Viscous Damper. Journal of Engineering Mechanics (ASCE), 2017; DOI: 10.1061/(ASCE)EM.1943-7889.0001354.

11. Priestley MN, Tao JR, Seismic response of precast prestressed concrete frames with partially debonded tendons PCI Journal, 1993; 38:58-69.

12. Somerville PG Development of ground motion time histories for phase 2 of the FEMA/SAC steel project. SAC Joint Venture; 1997.

13. G. C. Clifton, Development of perimeter moment resisting steel frames incorporating semi-rigid elastic joints. In: Proc. New Zealand National Society for Earthquake Engineering Conference. 1996; pp 177-184.

14. G C.Clifton, Semi-rigid joints for moment-resisting steel framed seismic-resisting systems, 2005; ResearchSpace@ Auckland.

15. G. A. MacRae, G. C. Clifton, H. Mackinven, N. Mago, J. Butterworth, S. Pampanin, The sliding hinge joint moment connection. NZSEE Bull, 2010; 43(3): 202–212.

16. B. Chiou, R. Darragh, N. Gregor and W. Silva, NGA project strong-motion database. Earthquake Spectra, 2008; 24(1): 23-44.